Journal of Theoretical Biology 259 (2009) 405–422

Contents lists available at ScienceDirect

Journal of Theoretical Biology

journal homepage: www.elsevier.com/locate/yjtbi

Vascular remodelling of an arterio-venous blood vessel network during solid tumour growth

M. Welter [a], K. Bartha [b], H. Rieger [a,*]

[a] Theoretische Physik, Universität des Saarlandes, PF 151150, 66041 Saarbrücken, Germany
[b] Department of Medical Biochemistry, Semmelweis University, Budapest, Hungary

ARTICLE INFO

Article history:
Received 20 December 2007
Received in revised form
26 February 2009
Accepted 3 April 2009
Available online 14 April 2009

Keywords:
Cancer
Tumour growth
Angiogenesis
Vascular networks
Blood flow
Computer simulation

ABSTRACT

We formulate a theoretical model to analyze the vascular remodelling process of an arterio-venous vessel network during solid tumour growth. The model incorporates a hierarchically organized initial vasculature comprising arteries, veins and capillaries, and involves sprouting angiogenesis, vessel cooption, dilation and regression as well as tumour cell proliferation and death. The emerging tumour vasculature is non-hierarchical, compartmentalized into well-characterized zones and transports efficiently an injected drug-bolus. It displays a complex geometry with necrotic zones and "hot spots" of increased vascular density and blood flow of varying size. The corresponding cluster size distribution is algebraic, reminiscent of a self-organized critical state. The intra-tumour vascular-density fluctuations correlate with pressure drops in the initial vasculature suggesting a physical mechanism underlying hot spot formation.

1. Introduction

Tumours can grow to a size of approximately 1–2 mm^3 before their metabolic demands are restricted due to the diffusion limit of oxygen and nutrients. In order to grow beyond this size, the tumour switches to an angiogenic phenotype and induces the development of new blood vessels mainly via sprouting angiogenesis, i.e. the formation of new vessels from pre-existing vasculature. This process is regulated by a variety of pro- and anti-angiogenic factors and is regarded as a prerequisite for further outgrowth of the tumour (Carmeliet and Jain, 2000). However, it has been suggested that many tumours can also grow in an avascular stage, mainly in well-vascularized tissue like brain and lung (Wesseling et al., 1994; Holmgren et al., 1995; Pezzella et al., 1997). Tumour cells (TCs) can grow along existing vessels without evoking an angiogenic response. This process was defined as vessel-cooption.

It was already proposed in Thompson et al. (1987) that tumours acquire their vasculature by incorporation of host tissue capillaries. The first detailed study of vessel cooption was published in Holash et al. (1999a), where it was found that 1 or 2 weeks after implantation of C6 glioma cells in a rat brain the small tumours were already well vascularized with vessels that had characteristics of normal brain vessels. After 4 weeks, blood vessels had undergone a dramatic regression without any compensatory angiogenic response. In the centre of the tumour, tumour cells were organized around the few functional vessels and massive tumour cell death was detected. In the tumour periphery, in contrast, a robust angiogenic response was observed. Vessel cooption has now been observed in different tumour types like human melanoma (Döme et al., 2002), neuroblastoma (Kim et al., 2002), and ovarian cancer (Zhang et al., 2003); it can persist during the entire period of tumour growth and it can even represent the only source for nutrients in angiogenesis-independent tumour growth (Sakariassen et al., 2006).

From these experimental observations the anatomy of solid, vascularized tumour grown within in a vascularized tissue displays a characteristic compartmentalization into essentially three regions (Holash et al., 1999a; Döme et al., 2002): (i) the highly vascularized tumour perimeter with a micro-vascular density (MVD) that is substantially higher than the MVD of the surrounding normal tissue, (ii) the well-vascularized tumour periphery with dilated blood vessels and a tortuous vessel network topology, and (iii) a poorly vascularized tumour centre with large necrotic regions threaded by only a few very thick vessels that are surrounded by a cuff of viable tumour cells. Thus, during tumour growth the original, hierarchically organized arterio-venous blood vessel network has been remodelled into a completely different compartmentalized morphology. Several microscopic phenomena on the cellular level have been identified to be involved in this remodelling process:

(1) *Angiogenic sprouting*: Up-regulation of pro-angiogenic factors in tumour-cells (like vascular endothelial growth factor, VEGF, and other growth factors) can create additional vessels via

* Corresponding author. Tel.: +49 681 302 3969; fax: +49 681 302 4899.
E-mail address: h.rieger@mx.uni-saarland.de (H. Rieger).

0022-5193/$ - see front matter © 2009 Elsevier Ltd. All rights reserved.
doi:10.1016/j.jtbi.2009.04.005

sprouting angiogenesis in some regions of the tumour, most frequently in its perimeter (Carmeliet and Jain, 2000). (2) *Vessel regression*: The maintenance of incorporated mature microvessels depends on the survival of endothelial cells (ECs) and their survival is intimately tied to their local microenvironment and, in particular, to the presence of pericytes, survival promoting cytokines, and extracellular matrix (ECM) proteins. The major molecular players that control this process are angiopoietins and VEGF (Holash et al., 1999a). Angiopoietin-1 (Ang-1) promotes EC survival and tumour vessel maintenance, whereas angiopoietin-2 (Ang-2) negatively interferes with these agonistic signals by blocking the Ang-1 receptor Tie-2 (Maisonpierre et al., 1997; Holash et al., 1999b; Scharpfenecker et al., 2005). In coopted blood vessels Ang-2 is up-regulated, causing the destabilization of their capillary walls, i.e. the detachment of pericytes from the endothelial tube (Holash et al., 1999b). Once ECs are separated from pericytes, they become particularly vulnerable resulting in the regression of destabilized vessels. (3) *Vessel dilation*: The vascularization program of the pro-angiogenic phenotype can be switched from sprouting angiogenesis to circumferential growth in the interior of the tumour. This switch is mediated by the guidance molecules EphB4 (and its ligand ephrinB2), both expressed by ECs of malignant brain tumours (Erber et al., 2006), which acts as a negative regulator of blood vessel branching and vascular network formation, and also reduces the permeability of the tumour vascular system via activation of the Ang-1/Tie-2 systems at the endothelium/pericyte interface.

The potential morphological consequence of these processes is (1) the increase of micro-vascular density (MVD) at the tumour perimeter (via up-regulation of VEGF and other growth factors), (2) vessel regression in the interior of the tumour (via up-regulation of Ang-2 and mechanical forces) and (3) vessel dilation and stabilization in the tumour centre (via VEGF and EphB4). The complex interplay of these three mechanisms with the architecture and blood flow organization of the original vasculature and a growing invasive tumour is the topic of this paper. By formulating and analyzing a mathematical model involving these features we will get insight into how they and their interplay affect morphological characteristics of the emerging tumour vasculature. Among these characteristics are the size, shape, MVD and blood flow distribution of the different compartments of the tumour (perimeter, periphery and centre), geometric properties of the tumour vasculature like the statistics and distribution of the spatial inhomogeneities and "hot spots" (regions of increased MVD and blood flow, Pahernik et al., 2001) within the tumour and drug transport along the intra-vascular blood flow.

In recent work (Bartha and Rieger, 2006; Lee et al., 2006; Welter et al., 2008) the issue of vascular remodelling in a growing tumour by the three basic mechanisms—angiogenic sprouting, vessel regression and dilation—was addressed in a model that comprised a regular capillary grid as initial vascular network. The compartmentalization of the tumour as well as other global features, like the time and radius dependencies of average MVD, tumour cell density, vessel radius and blood flow characteristics were predicted in good agreement with experimental data, but local characteristics, like a single hot spot in the centre and a general bias in the flow direction, could be attributed to the special topology of the initial network. In this paper we consider a more realistic arterio-venous vascular network as initial vasculature and study the effect it has on the emerging tumour vasculature.

In well-vascularized tissue the average inter-capillary distance is $50-100\,\mu m$, in highly vascularized tissue like brain even less (depending on the oxygen demand and the resulting diffusion length), implying the importance of the incorporation of the original vasculature into a model for tumour-induced angiogenesis. This vasculature is organized in a hierarchical way, in which an arterial and a venous tree are interdigitated by capillaries. Oxygen and other nutrients are distributed into the surrounding tissue by the lowest level capillaries, the two trees representing their supply and drainage system. The MVD, given by the average inter-capillary distance, is homogeneous in one kind of tissue to provide a homogeneous oxygen and nutrient supply, but the two interdigitating hierarchical trees form a spatially very inhomogeneous blood vessel network. Consequently the vascular remodelling process in a growing tumour will also be spatially inhomogeneous: sprouting angiogenesis occurs mainly from capillaries and venules, higher level arteries protected by a thick layer of pericytes are more stable and regress later or not at all, regression of higher level arteries has fatal consequences for the whole arterial sub-tree below it, newly formed vessels between arteries and veins could act as shunts redirecting huge amount of blood, etc.

1.1. Previous modelling

Mathematical modelling of tumour angiogenesis has been an active research area in the recent years, but there has been little work on the role of vessel cooption and regression. Since the early work of Balding and McElwain (1985), many models of the process of capillary formation in response to a tumour-derived growth factor have been constructed. Examples include Chaplain and Stuart (1993), Chaplain et al. (1995), Byrne and Chaplain (1995) and Holmes and Sleeman (2000). These models are macroscopic in that they deal with continuous quantities, such as endothelial cell density, via a system of partial differential equations. One disadvantage of this modelling approach is its inability to capture microscopic features of the process, such as vessel branching and looping and the morphological properties of the emerging capillary network.

Several researchers have therefore formulated discrete, or microscopic, models of tumour angiogenesis. These often contain a stochastic element and model at the level of the individual cell, see, for example Stokes and Lauffenburger (1991) and Turner and Sherratt (2002). Anderson and Chaplain (1998) derived a discrete model for EC movement in angiogenesis via a discretization of a continuous model. Here tip-cells located at discrete lattice points are assigned probabilities to migrate to adjacent lattice points within the next time-step. These probabilities account for chemotactic, haptotactic, and diffusive contributions corresponding to a continuum formulation. Capillaries are represented as masked points on the grid and probabilistic branching rules depend on the sprout age, VEGF concentration and EC density. An extension to three dimensions is presented in Chaplain (2000).

The blood flow in capillary networks has been modelled in Gödde and Kurz (2001), McDougall et al. (2002), Stephanou et al. (2005) and McDougall et al. (2006) and then extended to describe the dependence of vessel remodelling on blood pressure and shear stress (Gödde and Kurz, 2001; Bartha and Rieger, 2006; Lee et al., 2006; Stephanou et al., 2006; Welter et al., 2008). Recently discrete agent-based models for tumour-induced angiogenesis were coupled to models of tumour growth (Zheng et al., 2005; Bartha and Rieger, 2006; Lee et al., 2006; Frieboes et al., 2007; Welter et al., 2008; Wise et al., 2008; Macklin et al., 2008). A growing tumour coopting the vessels of the normal tissue was considered with a pre-existing static capillary network without angiogenesis or regression in Alarcon et al. (2003) and Betteridge et al. (2006) and with a fully dynamic capillary network in Bartha and Rieger (2006), Lee et al. (2006), Welter et al. (2008) and Owen et al. (2008).

1.2. Present model

1.2.1. Arterio-venous vasculature

To study and quantify these effects during vascular remodelling during tumour growth we employ and extend a mathematical model for a two-dimensional arterio-venous blood vessel network that has been presented in Gödde and Kurz (2001). Here we restrict our study to a two-dimensional situation, but it can straightforwardly be extended to three dimensions (to be published). The model generates stochastically an arterio-venous network with physiologically realistic parameters (Gödde and Kurz, 2001). By varying the number and location of sources and sinks the global topology of the network can be adopted to different situations for the initial nucleus of the tumour—e.g. close to a major artery or vein or far away from major vessels. At each branching point the vessel radius decreases according to Murray's law (Murray, 1926), each vessel represents a pipe with given radius within which blood flows according to Hagen–Poiseuille with a radius-dependent effective viscosity. Boundary conditions that imprint and define the blood flow in the network are the blood pressure values within the roots of the arterial and venous trees. The vessels represent the sources of the diffusion determined oxygen/nutrient concentration field, surrounding cells represent its sinks.

1.2.2. Sprouting angiogenesis

This arterio-venous network serves as the initial vasculature for our model of remodelling by a growing tumour. Depending on the local oxygen concentration tumour cells represent the sources of the diffusion determined VEGF concentration field, which triggers either the generation of tip-cells for angiogenic sprouting from existing vessels outside or at the periphery of the tumour, or the circumferential growth inside the tumour. In contrast to vessel in-growth models as in Anderson and Chaplain (1998) tip-cells are not dominantly generated by branching of existing tip-cells but by sprouting from vessels of the original network. This tip-cell generation from existing vessels is initiated by the activation of VEGF receptors with subsequent up-regulation of the delta-like-4 (Dll4) ligand in one EC (Liu et al., 2003), and the Dll4-mediated activation of Notch1 receptors in the neighbouring EC (Sainson et al., 2005; Williams et al., 2006). This lateral inhibition leads to an alternating pattern of cell fates in capillary walls under the influence of VEGF and results in a separation of one to two non-tip-cells between each tip-cell. The underlying negative feedback-loop involving VEGF receptors, Dll4 and Notch has been analyzed theoretically in Bentley et al. (2008), our model only incorporates the resulting pattern for tip-cell generation along existing vessels exposed to elevated concentrations of VEGF.

The subsequent migration, branching and anastomosis of angiogenic sprouts was recently modelled in a detailed way (Bauer et al., 2007; Milde et al., 2008), involving besides VEGF matrix metalloprotease (MMP) and the filamentous structure of the extracellular matrix. In our model tip-cells migrate in the direction of a sufficiently large VEGF gradient (chemotaxis), otherwise randomly. The path they describe is supposed to be filled with stalk cells forming a lumen and finally, once the tip-cell hits another vessel (anastomosis), a functional vessel carrying blood flow. These assumptions are analogous to previous work (McDougall et al., 2002, 2006; Stephanou et al., 2005), but some details differ: (1) Due to the pre-existing vasculature vessels typically migrate only $50-100\,\mu m$ before the filopodia of the tip-cell extending up to $20-30\,\mu m$ into the surrounding tissue in all directions (Gerhardt et al., 2003) touch another vessel. Therefore directional clues are not as important here as in pure vessel in-growth models. (2) Tip-cells migrate maximally $100-150\,\mu m$ and in case they did not make successful contact with another vessel, they retreat (Nehls et al., 1998). (3) Tip-cell branching is not included, but we allow for tip-cell generation along the sprout and the newly formed vessel, which mimics branching.

1.2.3. Vessel dilation and regression

Inside the tumour the VEGF concentration is generally still high but angiogenic sprouting is replaced by circumferential growth due to the up-regulation of EphB4 in the ECs forming the walls of coopted vessels (Erber et al., 2006). The molecular mechanisms for this up-regulation are unknown but apparently contact with tumour cells is necessary. Therefore we incorporate this switch to circumferential growth by a dependence upon the contact time of ECs with tumour cells.

In an analogous way we model the effect of an up-regulation of Ang-2 in coopted vessels, which has been analyzed theoretically in Plank et al. (2004) and which leads to vessel destabilization and regression: an increasing contact time of vessels with tumour cells, implying an increasing residence time within the tumour, leads to a higher collapse probability of tumour vessels. The collapse probability is also correlated with the origin of the vessel (artery, vein or capillary) and the shear force exerted by the blood flow upon the vessel walls. It is conceivable that mechanical forces in the form of solid stress exerted by the expanding tumour also influence the collapse of coopted vessels. This can in principle be included into the model along the lines described in Frieboes et al. (2007), Wise et al. (2008) and Macklin et al. (2008) but we choose here a stochastic approach: the tumour region with the potentially largest stress is the periphery due to the highest proliferation rate and because the necrotic centre consists of liquidized biological matter that generates a homogeneous interstitial fluid pressure, which is thus not able to sustain solid stress. Thus with increasing distance of a vessel from the tumour boundary not only its contact time with tumour cells increases (up-regulating Ang-2) but also the mechanical stress acting upon it. Hence the collapse probability of a coopted vessel increases with increasing distance from the tumour boundary (and with decreasing shear force).

1.2.4. Tumour model

Our focus in this work is the vascular remodelling process, which we assume to be dominantly dependent on where vessels are located, how stable they are (i.e. from which level in the arterio-venous tree they originate), how long they have been in contact with tumour cells and how well they are perfused. Therefore we choose a simplified representation of the growing tumour: proliferation of tumour cells takes place, if sufficient oxygen/nutrients are present and if there is available space. This captures the most essential features of experimental (Brú et al., 2003) and theoretical (Drasdo and Höhme, 2005) observations that proliferation of tumour cells is confined to the outer rim of an avascular tumour. Since in our model for vascular tumour growth proliferation depends on oxygen and since the oxygen concentration is highest close to vessels, tumour cells proliferate preferentially along vessels, which is commonly observed in aggressive tumours growing in vascularized tissue. We do not include migration of the tumour cells, but this can easily be incorporated into the model together with cell–cell adhesion and mechanical stresses (Ambrosi and Preziosi, 2002; Byrne and Preziosi, 2003; Breward et al., 2003; Frieboes et al., 2007; Wise et al., 2008; Macklin et al., 2008). Finally tumour cells die when they were underoxygenated for a specific time interval.

1.2.5. Scope and outline of this paper

The questions that we address with the model that we formulate are: What is the fate of the well-organized hierarchical

structure of an arterio-venous vessel network when it is co-opted and remodelled by an aggressively growing tumour? What are the geometrical characteristics of the emerging tumour vasculature and what are the potential mechanisms leading to spatial inhomogeneities or hot spots? And what are the global blood flow patterns and the drug transport performance of the tumour vasculature? Since we will be interested in the large scale properties of the vasculature of tumours with a size up to 5–10 cm, we will have to omit some of the mechanical and/or chemical aspects incorporated into other tumour-angiogenesis models that neglect the structure of the initial vasculature, and use a simplified, stochastic modelling approach instead.

This paper is organized as follows: in the next section the model is defined, including the method to construct an arterio-venous initial network. In the model definition we restrict ourselves to the mathematical formulation and refer to the introductory Sections 1.2.1–1.2.4 for the supporting biological observations and experimental literature. Section 3 presents the results for global properties for a choice of parameters that is guided by experimental data for melanoma (Döme et al., 2002). These results include a discussion of the emerging morphologies; radial distributions of vessel density, vessel radius, tumour density, flow rates, shear forces, vessel statistics, parameter dependencies, spatial inhomogeneities, and drug flow. Section 4 concludes the paper with a summary of the main results and a discussion.

2. Mathematical model

The model represents tumour cells and vessels as discrete elements which occupy lattice sites and bonds, respectively, on a two-dimensional triangular lattice (Fig. 1). Tumour and vessel network interact predominantly via a growthfactor (GF) and an oxygen concentration (O_2) field. Most of the mathematical definitions follow closely (Welter et al., 2008) apart from the arterio-venous initial network.

2.1. Definition of the system state

2.1.1. Tumour

Each lattice site of the space occupied by the tumour is identified with one TC. A lattice site which was occupied by a tumour cell in the past represents necrotic tissue, otherwise unoccupied sites represent normal tissue. The lattice constant of 10 μm is of the order of the typical size of a cell so that the identification of cells with sites is meaningful.

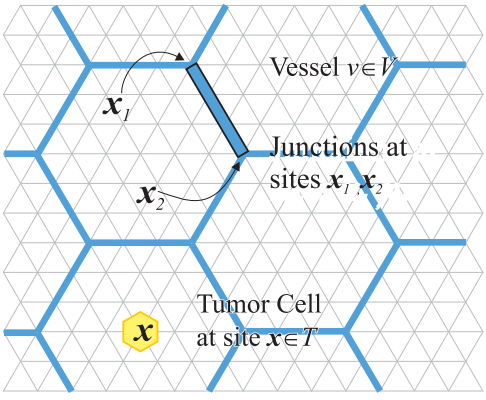

Fig. 1. Illustration of the discrete configuration space of the model: all discrete elements are aligned with the underlying triangular lattice shown in the background. Blue bars represent single vessels which occupy lattice bonds. One vessel is highlighted by a black frame, its junctions to other vessels are denoted by $\boldsymbol{x}_1, \boldsymbol{x}_2$. Each tumour cell (TC) occupies one lattice sites. A single TC is depicted as a yellow hexagon. (For interpretation of the references to colour in this figure legend, the reader is referred to the web version of this article.)

2.1.2. Vessel network

The vasculature is modelled as a network of connected ideal tubes that run along the bonds of the lattice. Its topology of which can be described by a graph, in which edges are identified with vessel segments. Graph nodes thereby occupy sites of the lattice. Due to the two-dimensionality of the model we allow individual vessels and TCs to occupy the same space within the lattice, since otherwise disconnected structures arise. In a three-dimensional model set-up this construction is not necessary. All elements (TCs, vessels, nodes) have physiological parameters associated with them—for instance vessel radius r—which define their internal state and which will be introduced below.

2.1.3. Blood flow

To compute the flow rate q of each vessel segment, the shear force f exerted on the vessel walls, and the blood pressure p, we adopt the approach widely used in the literature (Gödde and Kurz, 2001; Betteridge et al., 2006; McDougall et al., 2006): a system of linear equations is derived from Poiseuille's law and mass balance equations for the nodes, which is solved numerically to obtain the blood pressure for each node. At arterial/venous supply/drain boundary-nodes we set the pressure to fixed values. To account for the complex non-Newtonian fluid behaviour we use a vessel radius and hematocrit (red blood cell fraction)-dependent viscosity term (Pries et al., 1994). For simplicity we neglect the phase-separation effect and assume a constant hematocrit of 0.45 which is the average in humans.

2.1.4. Oxygen

The O_2 concentration field denoted as c is defined as the solution of the stationary (i.e. time-independent) diffusion equation $\nabla^2 c - \gamma_c c + \alpha_c(c^{(B)} - c) = 0$, where γ_c is a tissue-dependent consumption rate, $c^{(B)}$ the blood O_2 level and α_c the source strength incorporating local vascular area-fraction and wall permeability. It is solved numerically once per time step (see below), with no-flux boundary conditions on the lattice of the discrete system. We restrict ourselves to the stationary solution of the O_2-diffusion equation since the relaxation time of the O_2 concentration to adapt to source/sink changes is of the order of seconds whereas changes of the tumour or vasculature configuration occur on the time scale of hours. We further assumed that oxygen uptake is non-saturated so that a linear consumption term makes sense. In the presence of the high tumour demand this simplification is justified. We assume that all vessels have equal oxygen content and also contribute equally to tissue, i.e. α_c and $c^{(B)}$ assume constant values of model parameters at vessel sites.

Under physiological conditions only the thinnest capillaries release oxygen into the surrounding tissue, but in our two-dimensional situation also higher order vessels have to release O_2 because otherwise large scale depressions of the O_2 concentration would occur around large vessels due to the lack of capillaries, which would unrealistically confine tumour growth. This construct is again necessary due to the two-dimensionality of our model, in three dimensions the space around large vessels van still be filled with capillaries. We also implemented a three-dimensional version of the model, where only capillaries are a source of O_2. It turns out that the results are the same as in the present model in two space dimensions with also larger capillaries emitting O_2 (Welter et al., unpublished).

We also neglect variations of the O_2 level within the vessels, assuming these variations are small over the length of a O_2

releasing capillary. In previous work (Welter et al., 2008) we compared simulation results for models with constant and varying hematocrit and found differences only on a micro-scale but not in large scale characteristics.

2.1.5. Growthfactor

Analogous to the O_2 field we define the equation for the GF field denoted g. In practice it is calculated as the superposition of contributions from underoxygenated tumour cells, which are characterized by $c < c_{TC}^{(prol)}$, where $c_{TC}^{(prol)}$ is a model parameter. Each of these cells generates a GF distribution which decays linearly as $(1 - x/R_g)$ with the distance x up to the GF diffusion radius R_g. This is a simplification based on assumption that GF has a limited diffusion range similar to oxygen and that it is secreted at a constant rate.

2.2. Definition of the dynamical processes

The dynamical evolution of the system is described as a stochastic process in which elements can be removed or added and their internal state can be changed according to rates that depend on the current system state. In practice we implemented an iterative scheme where update rules that correspond to the processes described below are applied sequentially for each time step of length $\Delta t = 1$ h. A rate thus translates into a probability $p = \Delta t/\tau$ for a specific transition to happen within the time step of length Δt, where τ is the mean time between transition events. With our parameter choices, the probabilities are sufficiently small such that this approach is a reasonable approximation to a continuous stochastic process.

The microscopic biological observations for the following basic model assumptions were discussed in the introduction in Section 1.2, including the experimental citations.

TC Proliferation: (see Section 1.2.4) New TCs occupy empty neighbour sites of the existing tumour with probability $\Delta t/t_{TC}^{(prol)}$ if the local O_2 level is above the hypoxia threshold parameter $c_{TC}^{(prol)}$. The parameter $t_{TC}^{(prol)}$ is the mean proliferation time (Fig. 2a).

TC Death: (see Section 1.2.4) TCs are removed if the local O_2 level is less than the necrosis threshold $c_{TC}^{(death)}$ for longer than the time $t_{TC}^{(uo)}$, where $c_{TC}^{(death)}$ and $t_{TC}^{(uo)}$ are system parameters. For simplicity potential variations among different TC genotypes are neglected (Fig. 2b).

Angiogenic sprouting: (see Section 1.2.2) Sprouting can be initiated by the generation of tip-cells at sites on the vessel network depending on several factors:

(1) (VEGF dependence of tip-cell generation): The local GF concentration must be non-zero (for simplicity the sprouting probability is independent of the concentration value).
(2) (Alternating pattern of tip-cell and non-tip-cell in the vessel walls): There is no sprouting from the next $l^{(spr)}$ sites in the vicinity of existing branching points.
(3) (Switch from angiogenic sprouting to circumferential growth, see Section 1.2.3): When the tumour grows over a particular vessel-occupied site, sprouting is prohibited for this site after the delay time $t_{EC}^{(switch)}$.

If these conditions are fulfilled a new vessel segment may be added with probability $\Delta t/t_{EC}^{(sprout)}$, where the parameter $t_{EC}^{(sprout)}$ is the mean time to extend a sprout by the length of a lattice-bond. The direction along the steepest GF gradient is taken. During the following time steps more bonds are added—one per step with probability $\Delta t/t_{EC}^{(sprout)}$. For simplicity the direction from the initial bond is retained. On contact a branching point is created fusing the vessels and terminating the sprouting behaviour. Otherwise the extension of the sprouts is limited by the amount of time $t_{EC}^{(migr)}$, after which sprouts become inactive and count as normal (unperfused) vessels (Fig. 2c, d).

Vessel collapse: (see Section 1.2.3) We account for varying vessel stability by a "degree-of-maturation" variable w, which is initialized with the thickness of healthy vessel walls (see parameter section). w decreases continuously inside the tumour with the rate k_w. Vessels remain stable while w is larger than 0. In addition, collapses are correlated with shear stresses f on the

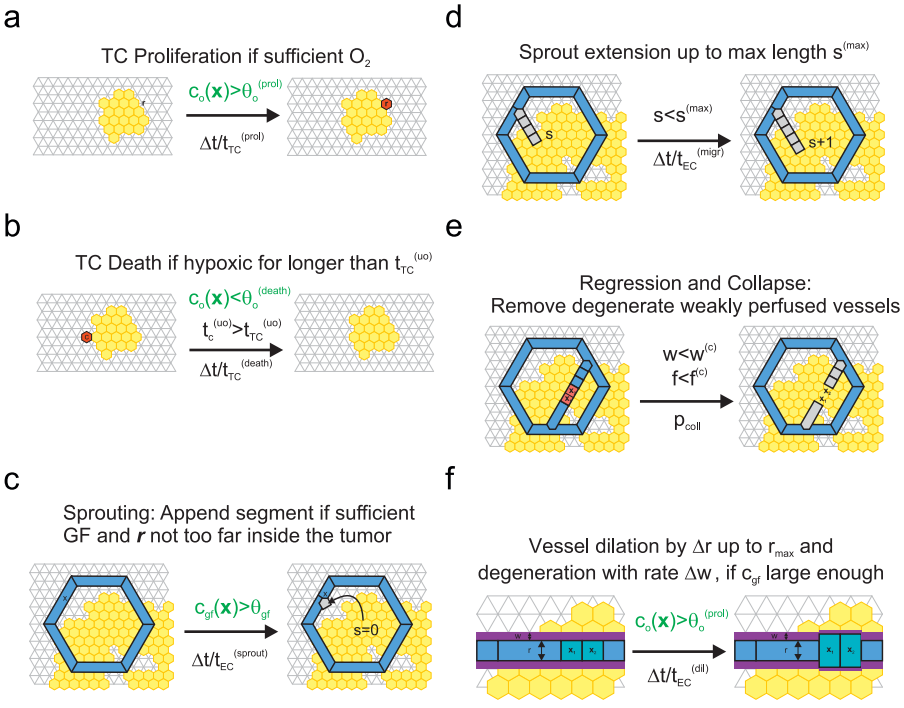

Fig. 2. Sketch of the dynamical processes in the model: (a) TC proliferation, (b) TC death, (c) sprout formation, (d) sprout migration, (e) vessel regression and removal, (f) dilation and wall degradation. See text for details.

vessel wall: if f is larger than the threshold parameter $f^{(coll)}$ vessels remain stable. Otherwise vessels are removed with probability $p^{(coll)} = \Delta t / t_{EC}^{(death)}$, where $t_{EC}^{(death)}$ is the mean survival time. Sprouts are an exception to the above mechanisms (Fig. 2e).

Vessel dilation: (see Section 1.2.3) After a vessel segment switched to circumferential growth (see angiogenic sprouting) the vessel radius r increases with the rate k_r if the local GF concentration is non-zero and $r < r^{(max)}$ (Fig. 2f).

2.3. Arterio-venous tree construction

Vasculature in real tissue exhibits a tree like structure. Few thick arteries branch out into arteriolar microvessels. Terminal branches are connected to the capillary bed, a dense network consisting of thin vessels where most of the exchange with the surrounding tissue happens. Further upstream blood is collected in venules which fuse into thick veins. The design goal of such a structure is to provide a sufficient supply of nutrients to all regions of the tissue, while minimizing the energy necessary to maintain the circulation.

Gödde and Kurz (2001) presented a method to grow and remodel vascular trees stochastically according to probabilistic rules that depend on local system properties. The simultaneous construction of arterial and venous trees makes their approach well suited for generating an initial vasculature for our tumour model.

Its basis is the growth of random arterial and venous trees on a lattice, under exclusion of already occupied sites. This is followed by stochastical shear stress guided remodelling at the tree leaves. Thereby weakly perfused leaves regress while strongly perfused leaves can grow. The vessel radii are computed by "Murray's Law" (Murray, 1926) from prescribed radii of the leaves. This eventually leads to a well-perfused space filling network with a relatively homogeneous capillary density distribution.

We provide the algorithmic details in the Appendix. Parameters are given there as well as in the parameter section below. Figs. 3a and 5 show the results used as input for our tumour model described above in Section 2.2.

While it is highly non-trivial to synthesize vascular networks that are realistic in every way possible, our initial networks exhibit reasonable hierarchical structures, spatial distributions of the capillaries, and good agreement with the flow-data of the original paper (Fig. 8).

2.4. Parameters

In order to observe typical features of the tumour-network morphology we have to simulate a sufficiently large area. The construction of the initial vasculature is carried out on a much coarser lattice because it is inherent to the algorithm that ca. 50% of the bonds are occupied with vessels. Therefore the resulting microvascular density is primarily a function of the lattice constant l_{coarse}. Based on the MVD for human skin (ca. 100 vessels per mm^2 cross-sectional area) and the MVD in the regular lattice cases (Bartha and Rieger, 2006; Welter et al., 2008), we set l_{coarse} to 60 μm. The a priori capillary radii are 4 μm for arterioles and 5 μm for venules, respectively. The radii of the vascular tree roots depend on the branching pattern. Because of this variation the blood pressure p at each root node is determined as a function of the vessel radius r: $p(r) = 0.133(18 + 72/(1 + \exp((r + 21\,\mu m)/16\,\mu m)))$ kPa, where r is negated for arterial vessels. It is based on the data in Pries et al. (1995), and results in average values of 2.4 kPa in vein (on average 88 μm radius) and 10 kPa in arteries (on average 52 μm radius).

Table 1
Model parameters of the base case.

Parameter	Value	Description
L	1200	Lattice size
l	10 μm	Lattice const
l_{coarse}	60 μm	Lattice const. (tree constr.)
$c^{(B)}$	0.45	Blood oxygen level
α_c	0.002 1/μm^2	O_2 source coefficient
γ_c (normal)	1/90^2 1/μm^2	O_2 consumption. coeff
γ_c (tumor)	1/50^2 1/μm^2	
R_g	200 μm	Growthfactor diffusion range
$t_{EC}^{(switch)}$	24 h	Sprouting/dilation switch delay
$t_{EC}^{(sprout)}$	5 h/10 μm	Sprout extension time
$t_{EC}^{(migr)}$	100 h	Sprout activity duration
$l^{(spr)}$	20 μm	Sprout sites minimum separation
$r^{(sprout)}$	4 μm	Initial sprout vessel radius
k_r	0.4 μm/h	Vessel dilation rate
$r^{(max)}$	25 μm	Maximum dilation radius
$t_{TC}^{(prol)}$	10 h	TC proliferation time
$t_{TC}^{(uo)}$	100 h	Hypoxic TC survival time
$f^{(coll)}$	1 Pa	Critical wall shear stress
$t_{EC}^{(death)}$	10 h	Unstable vessel survival time
k_w	0.04 μm/h	Dematuration (w) rate
$c_{TC}^{(death)}$	0.03	TC hypoxia O_2 threshold
$c_{TC}^{(prol)}$	0.3	TC proliferation O_2 threshold
	88 ± 21 μm	Venous tree root radius
	52 ± 14 μm	Arterial tree root radius
	2.4 ± 0.1 kPa	Venous tree root blood pressure
	10 ± 1 kPa	Arterial tree root blood pressure

Blood pressures and radii of the root nodes are stated as averages ± deviations over all configurations (see text).

In the following we define the parameters for a base case scenario for the tumour model (see Table 1). The size of the lattice is 1200×1200 sites, with the lattice constant $l = 10\,\mu m$ ($\approx 12 \times 10\,mm^2$ since it is a triangular lattice).

The initial tumour is an Eden-grown cluster of 1000 cells and 300 μm in diameter. We set the TC proliferation time $t_{TC}^{(prol)}$ to 10 h, the viability time under hypoxia $t_{TC}^{(uo)}$ to 100 h, and the apoptosis time to 2 h, the O_2-threshold for proliferation $c_{TC}^{(prol)}$ to $0.3 \approx 0.9\langle c \rangle$ and the threshold for extreme underoxygenation $c_{TC}^{(death)}$ to $c_{TC}^{(prol)}/10$.

We set angiogenesis related parameters as follows: sprout extension time (mean waiting time between additions of new lattice bonds to a sprouting vessel) $t_{EC}^{(sprout)}$ to 5 h, sprout viability time $t_{EC}^{(migr)}$ to 100 h (estimated from figures in Nehls et al. (1998)), sprouting site separation distance $l^{(spr)}$ to 20 μm, the initial sprout radius $r^{(sprout)}$ to 4 μm, the delay until the switch to circumferential growth happens $t_{EC}^{(switch)}$ to 24 h, the circumferential growth rate k_r to 0.4 μm/h, the maximum radius $r^{(max)}$ to 25 μm and the growth factor diffusion range R_g to 200 μm (estimated from morphological data by Döme et al. (2002)).

Parameters related to vessel regression are as follows: we set the critical shear force $f^{(coll)}$ deliberately to 1 Pa which is 10% of the average shear stress, and the mean waiting time for regression $t_{EC}^{(death)}$ to 10 h which applies for uncirculated as well as degenerate vessels ($w \leqslant 0$). We had to estimate the dematuration rate k_w from the presentation by Holash et al. (1999a). It is set to 0.04 μm/h, resulting in regression delays from 93 h (4 μm vessels) to 625 h (50 μm vessels). The maturation variable for the original vasculature and new sprouts is initialized with an estimate for the wall thickness (Pries et al., 2005).

The O_2-diffusion parameters are chosen so that the field becomes dimensionless, the diffusion range is ca. 100 μm, the O_2 level in the middle of two vessels drops to ca. 50% of the peak values. These are typical observations in Carmeliet and Jain (2000)

and Torres Filho et al. (1994). Our respective values are 0.002 $1/\mu m^2$ for α_c, $1/90^2\ \mu m^2$ for γ_c in normal tissue and $1/50^2\ \mu m^2$ in tumour tissue. An upper bound for the concentration is the blood oxygen level $c^{(B)}$ which we set to 0.45. The choice can be arbitrary because c scales linearly with $c^{(B)}$. We refer for a full discussion to Welter et al. (2008).

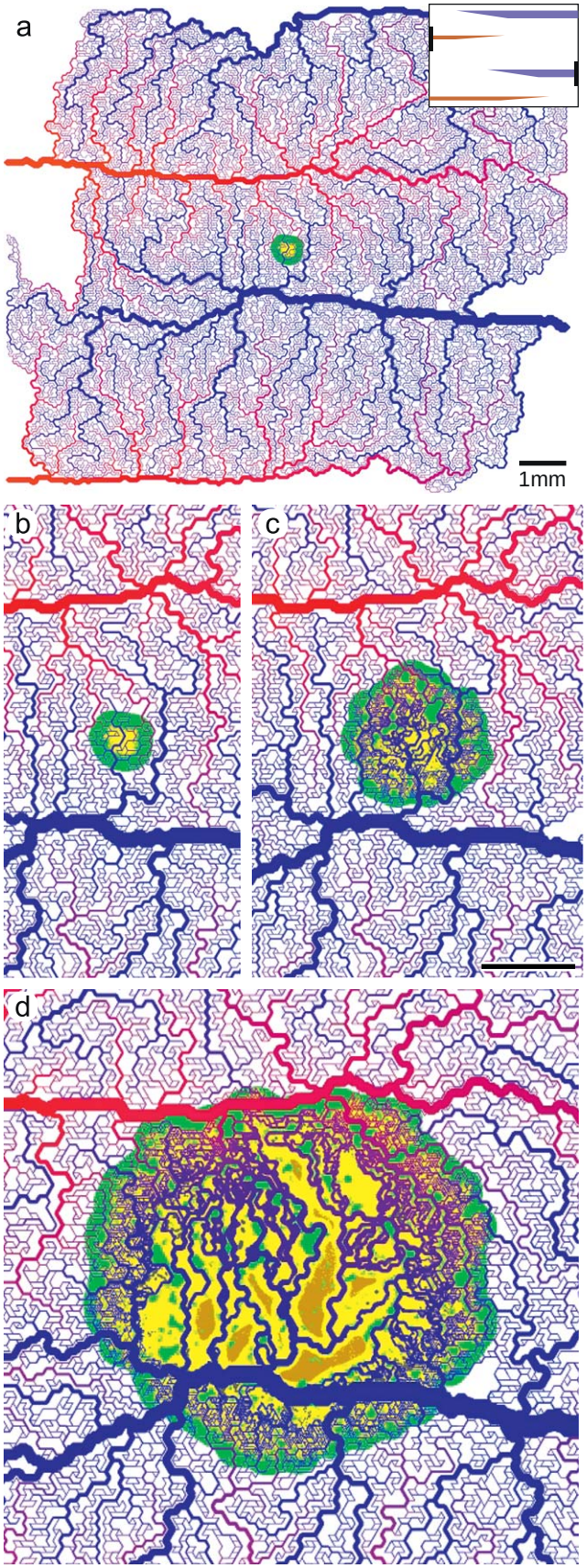

3. Results

The model predicts the dynamical evolution of the global morphology consistent with experiments and our previous results as explained in the introduction.

Fig. 3a shows a sample system in its initial state. The vessel network was generated by first laying out stems of the trees manually, and then starting the random growth process with branching points on each site on the stems. This is described in detail in the Appendix. The layout of the stems is indicated in the top right corner of Fig. 3. Their lengths and locations are sampled from uniform distributions. The approach was motivated by the observation that vasculatures exhibit relatively thick straight vessels down to a certain level in the hierarchy as can be seen in photos from the CAM (Mironov et al., 1998), or in recent 3d vascular imaging (Cassot et al., 2006) experiments.

Fig. 3b–d display snapshots at successive times. Initially the tumour O_2 consumption leads to decreased O_2 levels inside the nucleus and consequently enables vascular remodelling via growthfactor production of the TCs. The sprouting process first creates a dense capillary plexus which provides more oxygen and facilitates tumour growth. Vessel collapses begin after a few days (t =200 h). Small capillaries can collapse immediately under bad perfusion while thicker vessels survive longer due to their stability, i.e. large w, independent on blood flow until they become unstable. The network is thus progressively remodelled, predominantly within a thin band around the tumour boundary. The sparse network left in the centre remains static except for a few collapses of isolated threads.

The final configuration is displayed in Fig. 4a. A magnified view on the boundary region of the tumour is shown in Fig. 4b. The resulting network morphologies show the typical high-MVD periphery and low-density centre. The remaining internal vessels form short-cuts between arteries and veins which touch the tumour surface. This is a consequence of the dilation that all vessels undergo in the tumour. The short-cuts consist of neovasculature as well as parts of the initial vasculature. Beside isolated threads we frequently observe regions where vessels are densely clustered.

The configurations shown in Fig. 5 were generated from alternate layouts of the vascular stems which are illustrated again in the top right corner. The stems represent the sources and drains of the arterio-venous networks. Biologically they correspond to different arrangements of the number and location of the main arteries and veins in the original blood vessel network in the neighbourhood of the tumour nucleus. The

Fig. 3. (a) Snapshot of the initial model configuration. Arteries are red and veins blue. Their radius originates from the construction algorithms (Section 2.3), depending on the network topology and a priori capillary radii. The colour code of the resulting networks shows the blood pressure distribution from 12 (red) to 0 kPa (blue). The small yellow area in the system centre is the tumour nucleus initialized by Eden growth to a maximum of 1000 TCs. Necrotic tumour tissue which appears on the other figures has a dark yellow colour. The background in normal tissue/extracellular matrix is coloured green where the growthfactor (GF) concentration can cause angiogenesis. The inlet shows the layout of the vascular tree stems which serve as starting locations for the network generation algorithm. The lengths (indicated by wedge shaped part of the bars) and positions (indicated by the two black vertical bars) of these stems are drawn from uniform distributions. (b)–(d) Snapshots of the model evolution at times 0, 200, 600 h. The vessel network is progressively remodelled, resulting in the typical morphology with high peripheral MVD, dilated vessels, low central MVD with many isolated threads, cuffs of viable TCs around them, and necrotic tissue in non-vascularized zones. (For interpretation of the references to colour in this figure legend, the reader is referred to the web version of this article.)

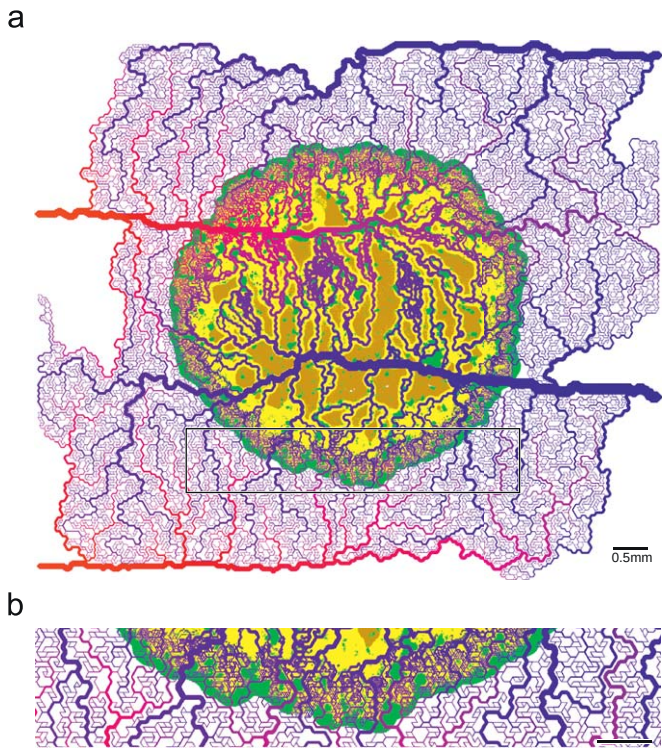

Fig. 4. (a) Final model configuration at $t=1200$ h resulting from continued expansion from the states depicted in Fig. 3. Typical features of solid tumour growth are retained. Now the tumour has also coopted a major artery and a vein. It is apparent that in between an increased number of well-conducting pathways have formed which serve as arterio-venous short-cuts. These originated from neovasculature as well as original capillaries which both have undergone circumferential growth and thus carry high blood throughput. The formation of clusters with increased local MVD, preferably close to the artery, is also evident. (b) Magnified view of the invasive edge that shows in detail how the vasculature is remodelled. Alternating with very high MVD on small scale, there are "holes" of the size of the intervascular distance in normal tissue. This is an effect of prohibiting sprouts from arteries, which would otherwise fill the holes, leading to a homogeneous vascular density. Behind the peripheral zone, the MVD drops rapidly. One can further see a few isolated dilated vessels directly connected to arterioles/venules in healthy tissue beyond the invasive edge.

result of the stochastic arterio-venous tree generation based on the different source and drain locations is shown in the top row. They look morphologically quite different, (a) displays a large artery close to the tumour nucleus, (b) a large vein, and in (c) is the tumour equally distant from major arteries and veins. However, the density of capillaries, the MVD, is identical for all three configurations.

Starting with these different initial networks the final tumour vasculature predicted by our model is depicted in the bottom row of Fig. 5. Obviously they differ in the local MVD configuration: in (d) the MVD is large in a central region (a hot spot), in (e) and (f) it is low. We conclude that differences in the original vasculature lead to differences in the arrangement of spatial inhomogeneities within the tumour (hot spots, necrotic regions), which will be discussed below. But the global compartmentalization pattern is identical for all three configurations, as can be seen from the radial distributions.

3.1. Radial distributions

Fig. 6 shows various quantities averaged over concentric annuli centred around the tumour centre. The stochastic construction of the initial vasculatures can leave the periphery unoccupied, but the vascularized regions exhibit a homogeneous MVD by design and have no holes. We run 10 Monte-Carlo simulations for each of the four basic layouts discussed above. We rejected configurations that were too small to support tumour growth till the end at $t=1200$ h.

MVD and TC density are computed as the fraction of occupied sites within a shell. Hemodynamic properties are averaged over occupied bonds only. MVD and vessel-radius show the typical compartmentalization that has been observed in melanoma (Döme et al., 2002) and glioma (Vajkoczy and Menger, 2000). We have discussed and compared our data extensively in earlier papers Bartha and Rieger (2006) and Welter et al. (2008).

Briefly, Döme et al. (2002) reported MVD and vessel radius in three distinct regions: the central region, a 100 μm wide peripheral band just behind the invasive edge, a 200 μm wide peritumoural region outside the invasive edge. In the central region, they found 25% MVD of normal tissue, and up to 200% in the peritumoural region. The vessel perimeter grows linearly from 50 μm and assumes a plateau at 200 μm by day 15.

In contrast to our simulation on a regular vascular network, flow rates and shear force now show a plateau similar to the vessel radius. Previously the fixed pressure gradient along the boundaries of the regular (rectangular or hexagonal) networks leads to unrealistic star shaped morphologies, directing all blood flow through the centre. Hierarchical initial networks do not lead to these artifacts. The axial blood pressure gradient dp/dl which is not shown here decreases monotonically towards the centre by more than one order of magnitude. The blood flow rate q is proportional to $r^4 dp/dl$ and increases on average towards the centre beyond a small local minimum at the invasive edge. Thus the r^4 dependency of the radius outweighs the pressure drop. The shear force dependency is rdp/dl which leads to a decrease towards the centre.

3.2. Vessel statistics

Fig. 7 shows scatter plots of hemodynamic variables against the vessel radius r, which are in good agreement with those obtained in Gödde and Kurz (2001). The plots combine samples throughout the vasculature (tumour and surrounding vessels) from all runs (at $t=800$). At this time a sufficient number of samples from the initial vasculature are available with negligible boundary effects.

We generally observe that the variance of the flow related parameters increases drastically towards the capillaries. This might be an artifact of our initial network construction, but averaged quantities display physiologically sound characteristics.

The dilation of internal tumour vessels leads to samples clustered at the maximum radius and one observes increased fluctuations at this particular radius. In particular vessels that connect arteries and veins at the tumour surface and thread through the tumour interior have blood pressure values in between the respective extremal values. In contrast, most non-dilated vessels which are obviously located in the outer rim fall in the same parameter ranges as normal vessels.

A few capillaries exhibit significantly lowered flow rates and velocities. Fig. 8, containing a spatial representation of the flow-rates, shows that the weakly perfused vessels are exclusively located in the tumour perimeter. As in this figure we observed that central vessels generally transport as much blood as equally thick vessels in normal vasculature. In Section 3.5 we show how this impacts the transport of drugs.

3.3. Parameter dependencies

We analyzed variations of all major model parameters extensively in Bartha and Rieger (2006) and Welter et al. (2008).

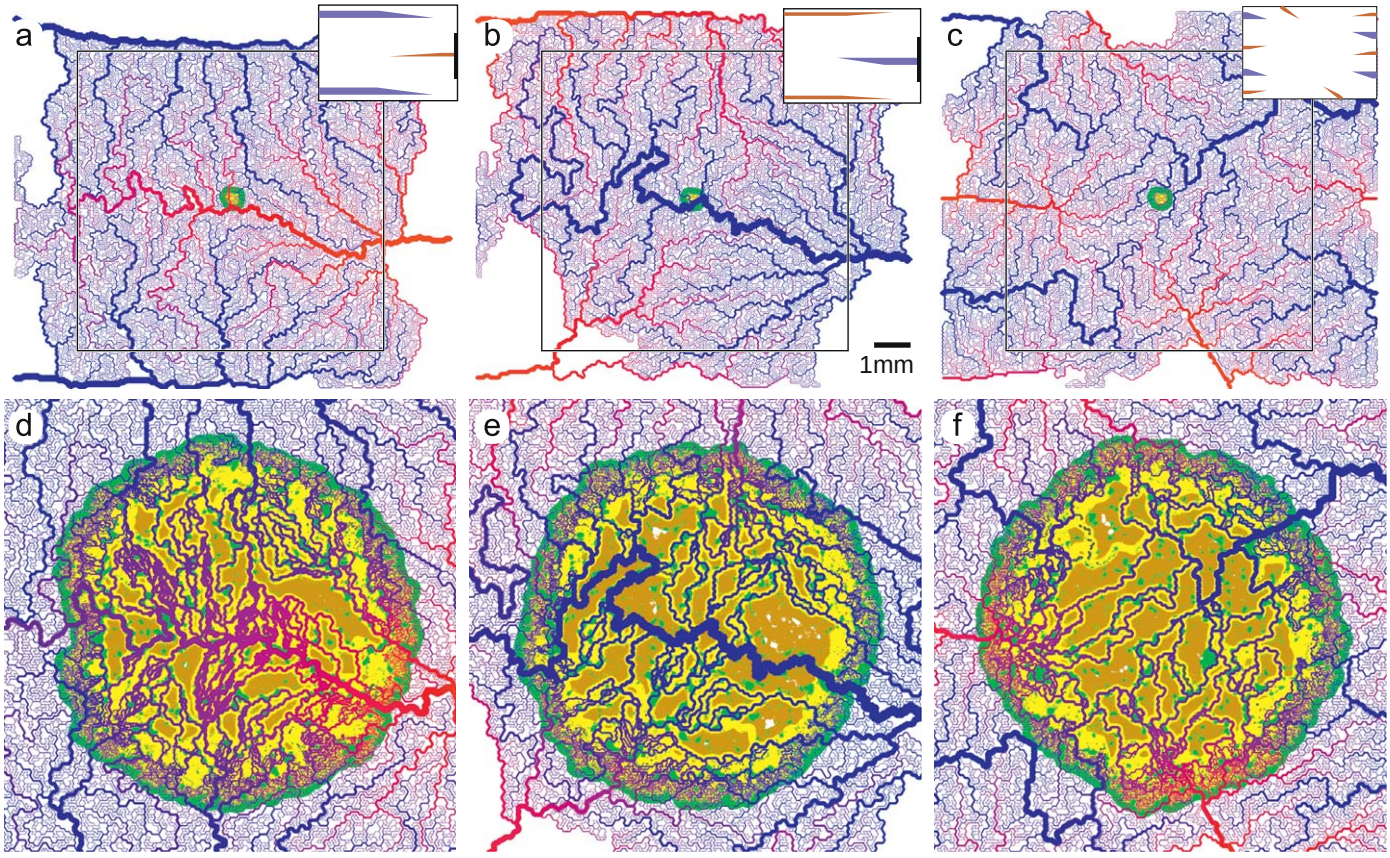

Fig. 5. (a)–(c) Initial vessel networks generated from different layouts as depicted analogous to the inlets in Fig. 3. (d)–(f) Final model configurations emerging from the networks above. The formation of local vessel clusters is clearly visible in the central region in (d), but not so in (e) and (f). In the latter increased MVD can be observed in a few locations close to the tumour boundary. In our reasoning, varying blood pressure differences between neighbouring vessels in the normal vasculature causes a highly inhomogeneous shear stress distribution in the tumour periphery. Thus the varying degree of stability leads to these clusters.

It was found that model predictions are very robust against variations and also details of the mathematical modelling. The effects of most parameter variations are obvious: the TC proliferation time $t_{TC}^{(prol)}$ mainly determines the expansion rate of the tumour provided the oxygen level c in the original vasculature is sufficiently above the proliferation threshold $c_{TC}^{(prol)}$. Otherwise growth can be slowed down depending on the rate at which peripheral vasculature is created and its final density (MVD). The latter is regulated by the sprout migration rate $1/t_{EC}^{(migr)}$ and minimum distance between branching points $l^{(spr)}$. The blood flow characteristics play an important role for the internal tumour MVD. The higher the shear stresses f (or the lower the associated threshold value $f^{(coll)}$) the more vessels will survive. We have identified a mechanism that leads to a lower bound for the MVD: when vessels collapse their blood volume is directed through the remaining vessels, increasing their flow rate and shear stress, thus stabilizing them. With the addition of the arterio-venous network the temporal evolution of the MVD depends on the vessel dematuration rate k_w. Once the tumour has grown over the peripheral plexus there is a delay until the maturity value w of vessels has decreased to 0. Together with the mean survival time $t_{TC}^{(death)}$ of degenerate vessels this delay causes the high-MVD rim to reach into the tumour by a certain width proportional to the delay time. Moreover the number of surviving thick arterioles and venules depends critically on the dematuration rate. If it is high these vessels will collapse early if it is low they may never collapse during the time of observation (1200 h).

The large shear force variations among capillaries in the original vasculature poses the question whether an absolute threshold for the collapse criterion is appropriate. Therefore we also checked the result of setting the probability $p^{(coll)}$, with which unstable vessels collapse, proportional to the relative deviation from the initial shear stress f_{init} ($p^{(coll)} \propto 1.0 - (f/f_{init})/f^{(coll)}$ for $f/f_{init} < f^{(coll)}$) instead of using an absolute threshold. This leads to decreased global MVD fluctuations among the simulation runs and also to increased local homogeneity, but does not change the model behaviour qualitatively.

In the present model variant, vessels can collapse any time after degradation ($w \leqslant 0$), depending on shear stress. It is, however, also an option to restrict collapses to the tumour rim. For example, it has been suggested that the death of tumour cells releases solid pressure from near vessels that is otherwise exerted by the tumour (Griffon-Etienne et al., 1999). Moreover, in previous papers we assumed the existence of a stable radius, preventing collapses in the centre where vessel radii are larger. Indeed, the EphB4 signalling mechanism which induces circumferential growth also leads to reduced leakiness, tightened EC junctions and endothelium/pericyte interaction (Erber et al., 2006), making an actual stability improvement plausible. Therefore we altered the model, assuming unconditionally stable internal vessels, by choosing collapse probability $p_{ring}^{(coll)}$ which takes on $p^{(coll)}$ only inside a band of width $l_{ring}^{(coll)}$ centred at the invasive edge, and which is zero otherwise. The result depends strongly on the time vessels spent in the collapse region, given implicitly by $l_{ring}^{(coll)}$ divided by the radial expansion velocity of the tumour. If this time is of the order of the survival time inside the tumour a transition occurs towards a highly vascularized centre, shown in Fig. 9 and analyzed in detail in Bartha and Rieger (2006) and Welter et al. (2008). Moreover $p_{ring}^{(coll)}$ causes less fluctuations with respect to initial networks because more of the initially thick vessels can

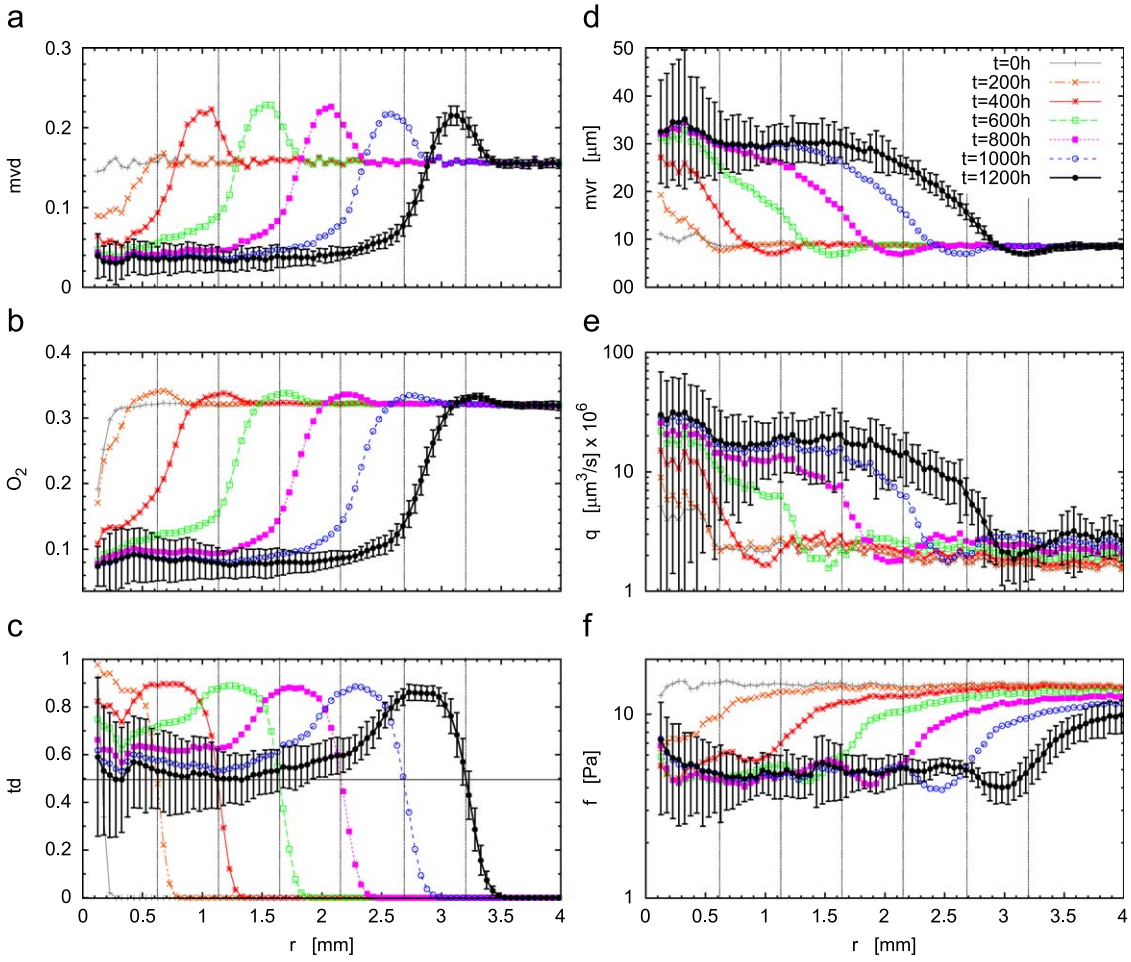

Fig. 6. Radial distributions of hydrodynamic and morphological variables of the base case simulations. The radius r here denotes the distance from the tumour centre. One data point represents an average over a concentric 50 µm wide shell, and over 40 runs: (a) shows the MVD, (b) the O_2 level and (c) the TC density, (d) the vessel radius, (e) the flow rate and (f) the shear force. The latter three are given as the average over actually occupied sites within a shell, instead of over all sites. For $t = 1200$ h also the root mean square deviations are indicated as error bars.

provide a backbone which never collapses due to $w > 0$ while being in the collapse ring.

3.4. Spatial inhomogeneities

Qualitatively one can already see that the location of highly vascularized zones in the tumour is connected to the location of the thicker vessels. They occur frequently where an artery is close to a vein, or vice versa, since an increased number of vessels survive in between. This can be seen clearly in Fig. 4 but it is also apparent in other configurations (Fig. 5). Qualitatively we can explain those hot spots through blood pressure gradients that arise in the tumour vasculature when short-cuts between nearby arteries and veins are formed. Major vessels can thereby act as stable backbones with very high or low blood pressure. Close proximity of two or more such vessels implies high shear stresses in the intermediate capillary bed and thus increased stability. Moreover the shear stress in arteries is normally larger than in veins. This asymmetry apparently leads to hot spot formation preferably close to the arterial branches.

This motivates the following quantitative analysis where intervascular "blood pressure" gradients of the original vasculature are related to the tumour MVD: first we compute a field $p(\boldsymbol{x})$ as solution to the Laplace equation $\nabla^2 p = 0$ subject to the boundary condition that p is set to the blood pressure at vessel sites. Thus p interpolates the blood pressure between adjacent vessels. Then, for a given region, we obtain the spatial average of the gradient $\|\nabla p\|$ at $t = 0$ h and plot it against an estimate for the tumour MVD at $t = 1200$ h.

The main plot of Fig. 10 shows the MVD versus $\langle\|\nabla p\|\rangle$ over entire tumours with one data point per simulation run. The correlation coefficient is usually very large ≈ 0.9 for this global measurement. Analogously we analyzed single tumour instances where the average is taken locally over randomly distributed discs with 150 µm radius. The inset shows the resulting distribution of one such measurement. The correlation coefficients of which vary between 0.2 and 0.4. Since a single collapse event can cause long-ranged regressions of adjacent network sections, it is plausible that local measurements only show weak correlations. Moreover since the vascular blood pressure at boundary vessels is prescribed based on their radius, only the location of initial vessels leads to the variety of emerging tumour morphologies.

Fig. 11 shows intermediate data which stems from the simulation run shown in Fig. 4. The bottom image (Fig. 11c) shows the site occupation by the vessel network. It is easy to identify the tumour network by its typical structure. In Fig. 11a, where $\|\nabla p\|$ is displayed, one observes that indeed the local gradients are stronger in the area close to the major artery in the top half, than close to the vein in the lower half. The snapshots (b)

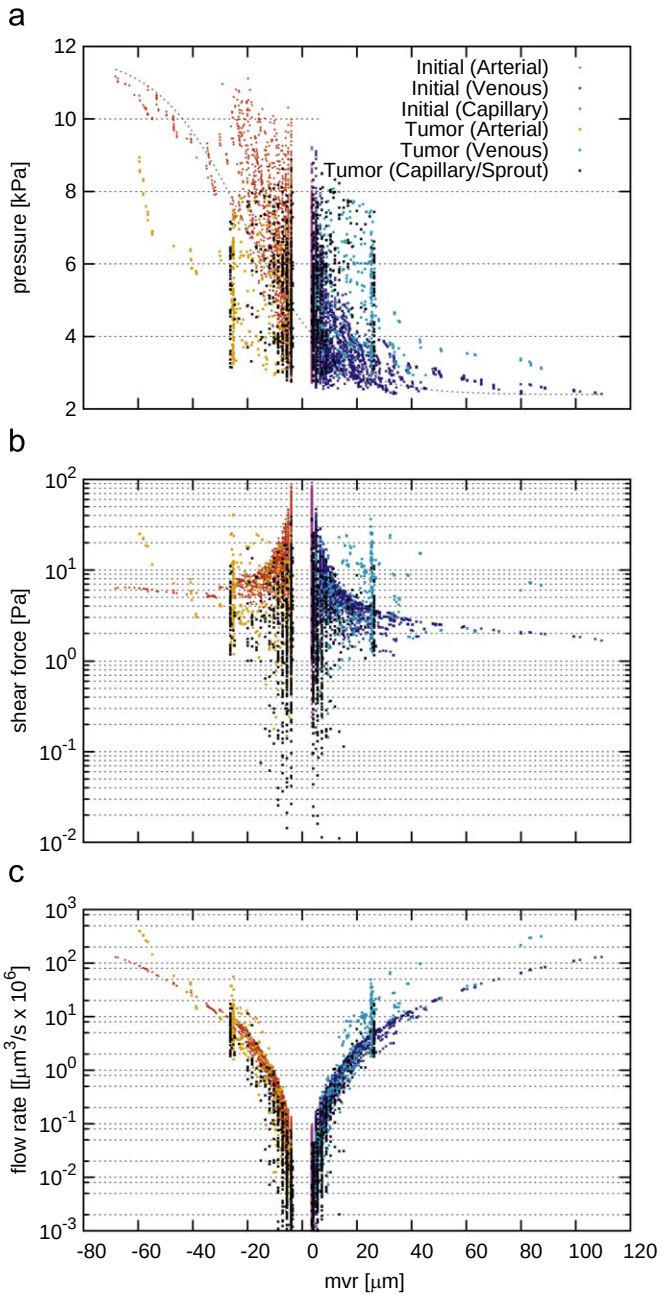

Fig. 7. Scatter plot showing hydrodynamic variables of a single simulation run plotted against the vascular radius. Each data point is a sample from uniformly distributed locations over the entire network. Samples from arteries are red and plotted with negative radius, capillaries are pink, veins are blue, all drawn from the original vasculature at $t=0$ h. Black dots represent samples from the tumour vasculature of base case at $t=1000$ h. Since tumour vessels have no hierarchical organization, these points were put with probability 1/2 on one side or the other. (For interpretation of the references to colour in this figure legend, the reader is referred to the web version of this article.)

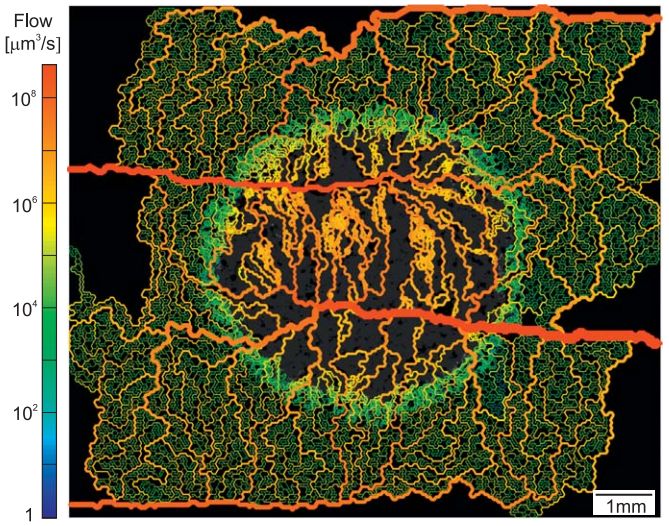

Fig. 8. Flow rate distribution in the vessel network shown in Fig. 4 with a logarithmic scale. The flow rate here is the blood volume per time through the vessel cross-section, not to be misunderstood as the blood flow per tissue volume. In our results dilated tumour internal vessels usually exhibit high flow rates like in this instance. If one would measure in/outflow per tissue volume element as in dynamic MRT measurements one would observe hot spots located at the respective high-MVD zones.

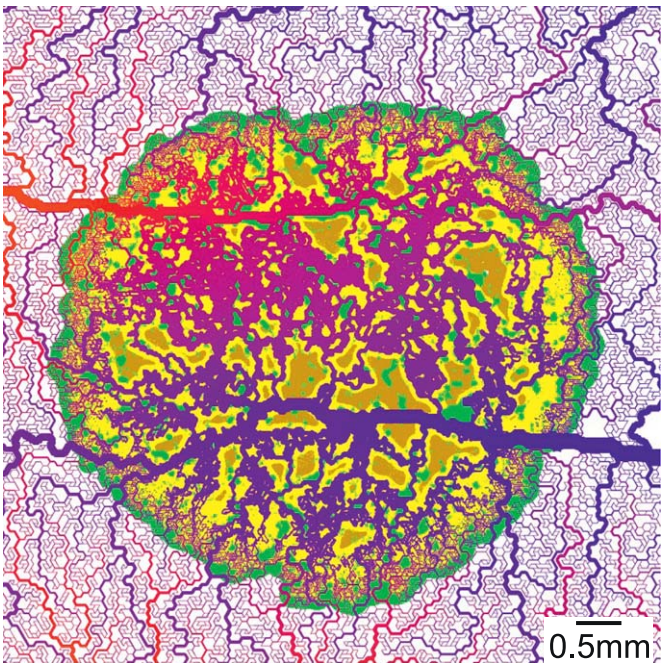

Fig. 9. Final configuration at $t=1200$ h of a simulation run using an alternate vessel collapse rule where vessel collapses are restricted to a thin band (here 400 μm in width) around the invasive edge. The new collapse probability $p_{ring}^{(coll)}$ equals $p^{(coll)}$ modulated with a window-function which depends on the distance to the tumour centre (see text). In this instance, parameters are such that the mean survival time of unstable vessels is of the order of the time they spend in the "collapse region". This puts the random collapse process in a dominant role over the maturity variable. The system is near a transition to a fully vascularized tumour. The parameter set is the same as in the base case, except for the critical shear force $f^{(coll)}$ which is set to 3 Pa, instead of 1 Pa.

and (d) on the right column show respective averages of the left-hand side data. These distributions show the behaviour that zones with elevated $\langle\|\nabla p\|\rangle$ are also probable locations of high MVD.

We further quantify the spatial inhomogeneities by probability distributions for local MVD (Fig. 12a), necrotic region size (b) and hot spot size (c). The distributions are determined by histograms of the respective local samples, combined from 40 runs. The MVD is estimated as the fraction of occupied sites within boxes (250 μm in size) of a regular grid. The plot displays two peaks. One large peak at low MVD ≈ 0.07 which decays algebraically with exponent ~ 1.4 and a smaller peak at MVD ≈ 0.45. The latter originates from the high-MVD zone in the tumour periphery. Not included is a peak which appears at MVD $= 0$ due to large non-vascularized regions. The necrotic-region size distribution shows the probability to find a cluster of dead TCs with a given cell

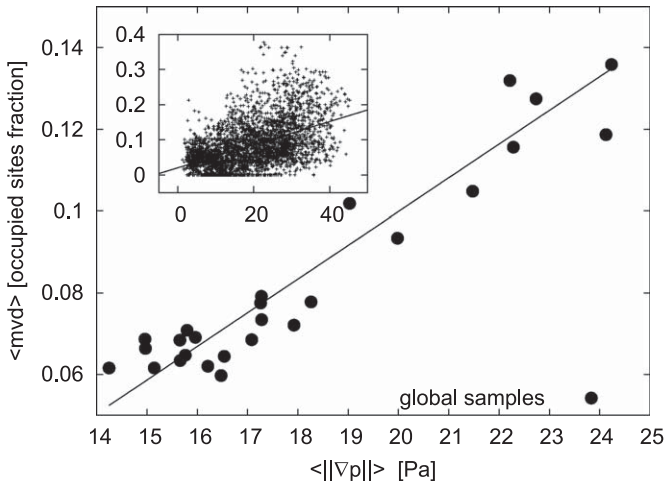

Fig. 10. Vascular density versus the mean pressure gradient $\langle|\nabla p|\rangle$ originating from the blood pressure differences between neighbouring vessels (see text). In the main plot data points stem from different runs of the base case, whereby the averages are taken over the entire tumour interiors (excluding the vascularized boundary region) at $t = 1200$ h. The inset displays data for a single tumour, where the averaging is done locally over a small disc with radius 150 μm (see Fig. 11).

count. The hot spot size distribution plots the probability to find a cluster with a certain number of sites where the local MVD is larger than a threshold (here 0.15). Both of the latter distributions exhibit purely algebraic decay also with the exponent ~1.4.

3.5. Drug transport

To analyze the effectiveness of blood-borne drug transport to a tumour and its distribution inside a time-dependent concentration profile over the vasculature is propagated according to the local blood flow rates. A corresponding mathematical model was presented (McDougall et al., 2002) for a pure vessel-in-growth capillary network, originating from a single parent vessel. It was predicted that large amounts of drug bypasses the tumour, varying by an order of magnitude depending on parameters. We adopt this method to check whether there are similar obstacles to successful drug delivery inherent to the tumour vascular networks, predicted by our model.

The starting point is a given configuration for the vasculature with precomputed variables for flow, flow velocity, vessel length, and radius. In addition, a mass parameter m is now associated with each vessel describing the amount of drug in the blood

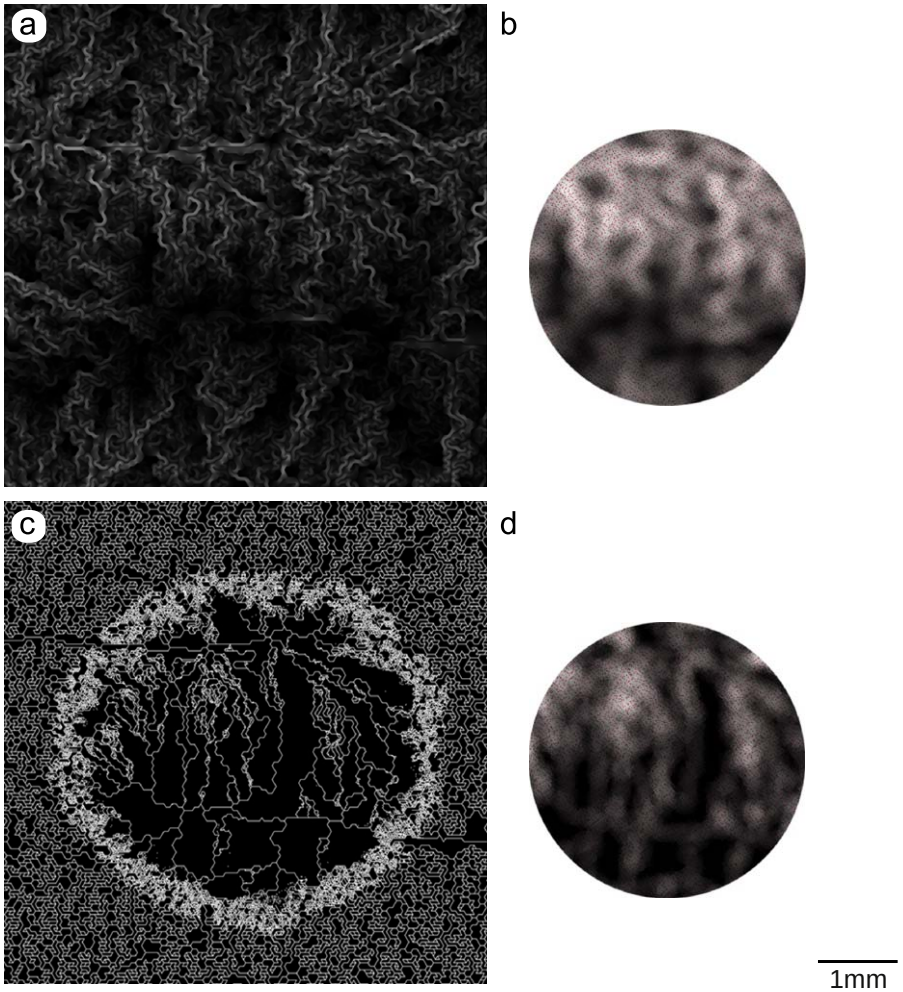

Fig. 11. Demonstration of the intermediate data that lead to the plots in Fig. 10: (a) shows the local magnitude of the gradient $\|\nabla p\|$ (see text). To correlate the MVD locally with $\|\nabla p\|$, mean values where computed at randomly distributed locations, each by averaging over a 150 μm radius disc; (b) shows these samples, such that space closest to some data point is filled with a grey scale value proportional to $\langle\|\nabla p\|\rangle$; (c) shows the site occupation of the vasculature; (d) shows an estimate for the local vascular density. Value ranges are 0–45 (black to white) for $\|\nabla p\|$ and 0–0.4 for the MVD.

volume contained in the vessel. The mass content m is deterministically updated in successive time steps as follows: first the drug amount flowing out of vessels is determined and added to respective node-mass variables. Under the assumption of perfect mixing, the nodal masses are then redistributed into further downstream vessel. Thereby mass conservation is strictly enforced. A detailed description can be found in Welter et al. (2008) and McDougall et al. (2002). The most severe limitation of this model is that there is no exchange with extra-vascular space and therefore also no uptake by the tumour.

The results in the following were obtained with a continuous injection into our base case vasculatures. From $t = 0$ on, blood with solute drug at conc. $C^{(init)} = 1$ flows into the vasculature which is initially filled with "clean" blood. The flow rates are of the order of mm/s, which is sufficient to saturate 80–100% of the vessels within seconds, depending on the network configuration.

Fig. 13 shows a sequence of snapshots over 6 s. Drug enters the system via the arteries and flows downstream with a sharp transition at the drug/clean interface. When vessels merge in upstream direction mixing with clean blood occurs so that the concentration profile smooths out in the veins. After 20 s nearly full saturation is achieved. Dilation of internal tumour vessels and direct connections to feeding arterioles lead to comparably fast filling with drug. The torturous structure and the redirection of blood flow through shot-cuts, away from the capillary bed, leads to decreased flow rates in the periphery. Figs. 7c and 8 show such vessels with low flow rates of the order of $10^3\,\mu m^3/s$, corresponding to velocities of the order of $10\,\mu m/s$. The average flow velocity over all vessels in the original network is $\sim 1.8\,mm/s$. Consequently we frequently observe regions which take significantly longer to be filled.

Quantitative analysis of drug efficiency impact is only possible to a limited degree due to the lack of tumour uptake modelling. Moreover even few surviving TCs can grow a new tumour mass. Nonetheless we measured statistics for the total amount of drug in the vasculature. Fig. 14a shows the fractional length of the tumour vessel network for which the maximum drug concentration was larger than indicated on the c-axis. After 20 s,

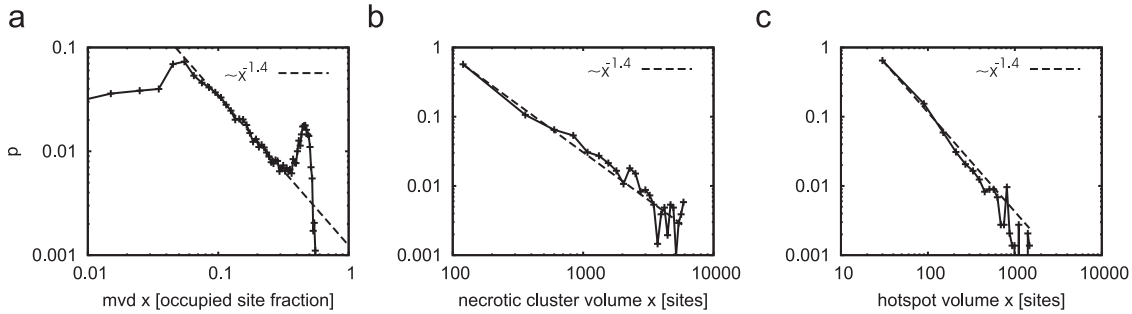

Fig. 12. Probability distributions in log–log plots, for (a) the local MVD, given as the local average over 250 μm wide boxes, (b) the volume of necrotic tissue clusters, defined as the number of sites in connected components of dead tissue, (c) the volume of vessel hot spot areas, defined as the connected components of regions where the local MVD exceeds a threshold (0.15). The distributions are generated by binning observed values in histograms over 40 simulation runs (at $t = 1200$ h). We note that the distributions show algebraic decay. In this instance in particular with the same exponent with an error of 2%.

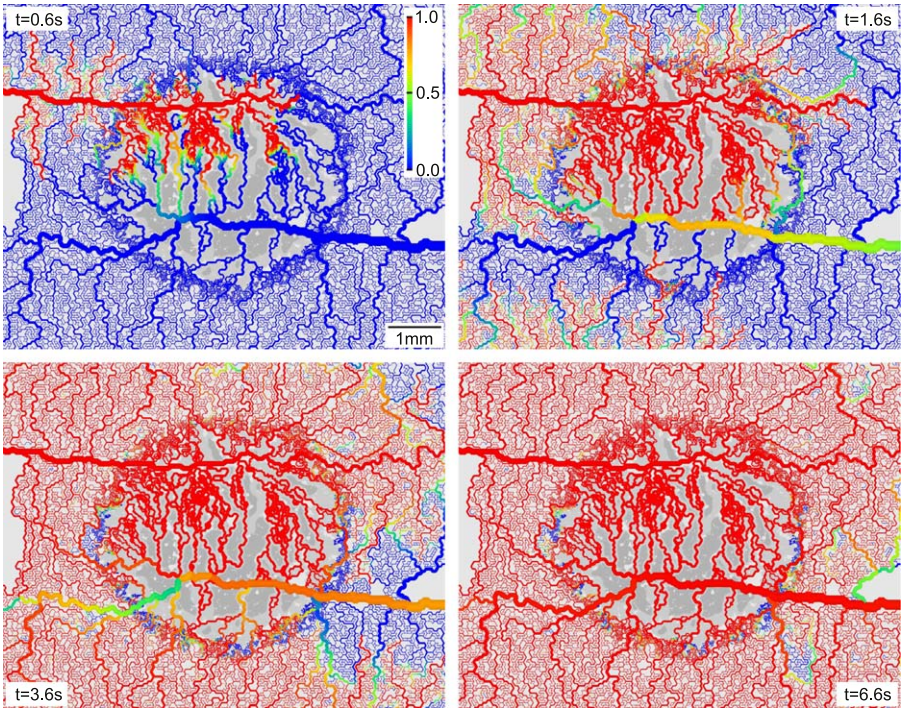

Fig. 13. Snapshots of the drug-flow simulation using the basic configuration (Figs. 3 and 4) at $t = 1000$ h. The colour code shows the drug concentration as indicated on the gradient bar. A high drug concentration reaches most parts of the vasculature after a few seconds. In the $T = 6.6$ s snapshots a few vessels in the boundary region are not yet perfused. The time until drug saturates the complete vasculature is of the order of minutes. We can observe this behaviour generally for all resulting networks.

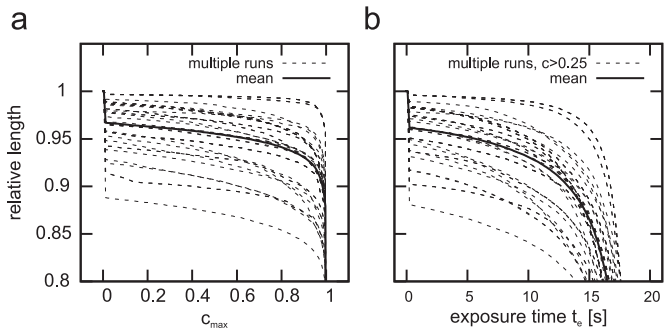

Fig. 14. (a) Fraction of total tumour network length that has been exposed to a drug concentration larger than the indicated concentration c_{max} (at $t = 20$ s of the drug simulation). The black line represents the average over 40 runs with different networks. (b) Fraction of total tumour network length that has been exposed to a drug concentration larger than 0.25 for longer than indicated time t_e. The black line represents the average over 40 runs with different networks. Like in Fig. 15, tumour networks from the base case at t =1000 h were used.

on average $94 \pm 3\%$ of the vasculature had been exposed to a drug concentration of at least 80%. For higher concentrations the curve decreases drastically. The curve at $c = 0$ shows that $4 \pm 3\%$ had not been drug perfused at all. In absolute numbers the latter corresponds to 15 ± 12 mm. Fig. 14b shows the fractional length of the tumour vessel—network for which the concentration was larger than the threshold $c = 0.25$ for a total duration greater than indicated on the x-axis as t_e. This measurement was also done at $t = 20$ s, thus the exposure time cannot be longer than that. It shows that large parts, say $93 \pm 4\%$, of the vasculature had been exposed to 50% drug concentration longer than 10 s. Considering the flow rates/velocities mentioned above one can expect the remaining few millimetres to be drug perfused within a time frame of minutes.

4. Conclusion

4.1. Summary

In this paper we formulated a hybrid cellular automaton model to analyze the vascular remodelling process of an arterio-venous vessel network during solid tumour growth. It is based on the modelling approach described in Bartha and Rieger (2006), Lee et al. (2006) and Welter et al. (2008) and extends it by incorporating a hierarchically organized initial vasculature comprising arteries, veins and capillaries. The model involves sprouting angiogenesis, vessel cooption, dilation and regression as well as tumour cell proliferation and death.

The model predicts that the tumour vasculature emerging from the interplay of these processes is non-hierarchical and compartmentalized into a highly vascularized tumour perimeter, a tumour periphery with large vessels density and dilated vessels and a central region containing necrotic regions with a low microvascular density threaded by extremely dilated vessels. This tumour compartmentalization is therefore independent of the initial vasculature, as has been conjectured on the basis of results for models involving a grid-like initial blood vessel network (Bartha and Rieger, 2006; Lee et al., 2006; Welter et al., 2008). Blood-borne drug transport along the tumour vasculature also turns out to be efficient, the reason for it being the dominant regression of vessels with low shear-forces leaving only those that are well perfused.

One consequence of the arterio-venous initial vasculature, which is absent for grid-like starting networks, is the emergence of short-cuts or "shunts" and concomitantly an increased blood flow through the tumour vasculature. There are experimental studies which agree with this prediction: in Sahani et al. (2005) perfusion parameters in rectal cancer were measured via computer tomography where consistently increased blood flow is reported by approximately a factor of two compared to normal tissue. It was argued that angiogenesis facilitates the creation of arterio-venous shunts which bypass the capillary network. The same mechanism is at work in our model: thick arterioles and venules provide a well-conducting support structure around the tumour. Since the total pressure difference between the tree roots is fixed, the transported blood volume is given by the total flow resistance of entire vascular tree. Dilation of a few vessels forming a path between the tree roots can remove bottlenecks formed by thinner vessels. The creation of new vessels thereby promotes arterio-venous short-cuts, or shunts, through multiple partly disjoint paths. After vessel dilation this leads to a decreased total flow resistance, which implies an increased blood flow through the tumour vasculature when compared with the initial vasculature. This is in contrast to grid-like initial networks, where the total flow resistance is dominated by the network outside the tumour (Bartha and Rieger, 2006; Welter et al., 2008) and the flow cannot increase via the dilation of tumour internal vessels.

Another consequence of an arterio-venous initial vasculature is the emergence of isolated highly vascularized clusters connected by thick vessels within the tumour vasculature. These "hot spots" are also observed in real tumours (Pahernik et al., 2001). Already by a visual comparison of the starting network with the final tumour vasculature one observes that hot spots form more frequently in those regions where the starting network contained predominantly arteries. An analysis of the correlations between various local hydrodynamic quantities of the original network (blood pressure, blood pressure gradient, blood flow) and the local MVD in the tumour vasculature revealed a significant correlation between local blood pressure gradients of the original arterio-venous network and the most probable locations of hots spots in the tumour vasculature. This is plausible since a high pressure gradient within the vessels implies a high shear force exerted by the blood on the vessel walls, which stabilizes the vessel against collapse and therefore leads to an increased vessel survival probability when the tumour has grown over this region. We note that in our model this hydrodynamic mechanism plays a dominant role in the hot spot formation, whereas potential local variations in pro- and anti-angiogenic effectors within the tumour were not involved but could also play a role in this process. It should be possible to check the model predictions experimentally by implanting a tumour nucleus into healthy tissue, whose vasculature has been analyzed before implantation.

We also find that the emerging spatial inhomgeneities in the tumour vasculature are organized in a complex way: the probability distribution of local MVD values as well as the probability distribution of the hot spot volume (defined as the size of connected clusters of regions with MVD larger than the original MVD) has an algebraic tail with exponent $\sim$1.4. Also the size distribution of the connected clusters of necrotic tumour regions showed an algebraic tail (again with exponent $\sim$1.4). These power laws are reminiscent of a self-organized critical state (Jensen, 1998), for which the absence of a typical length scale (over which for instance size distributions would decay exponentially) is characteristic, like in a stochastic dilution process at the percolation threshold or a flow-correlated percolation process (Lee et al., 2006).

4.2. Discussion

We summarize briefly what biological insights we can extract from our work. (a) The experimentally observed compartmentalization of the tumour vasculature (Holash et al., 1999a; Döme et al., 2002) is independent of the initial vasculature and a consequence of the basic mechanisms that we identified: (1) the existence of an original vasculature, (2) angiogenic sprouting in the tumour perimeter, (3) blood flow correlated vessel regression and (4) a switch from angiogenic sprouting to circumferential growth within the tumour. If the latter is absent, thick vessels will be rare, leading to increased shear flow and concomitantly to increased stability of the tumour vessels—thus altering the compartmentalization. In addition we predict that (b) blood-borne drug transport is efficient through a tumour vasculature in which vessel regression is blood flow correlated—experimentally observed deficiencies in drug delivery must have other reasons. And (c) the experimentally observed hot spots or MVD inhomogeneities of the tumour vasculature are correlated with the blood pressure gradients of the original vasculature.

Potential experimental tests for these predictions are: (i) if it would be possible to experimentally switch off circumferential growth or prevent vessel collapse the model predicts a different compartmentalization of the tumour vasculature, which could be analyzed experimentally with immunohistology; (ii) intravital microscopy with fluorescently labelled drug proteins or nanoparticles could be used to check the model predictions on blood-borne drug transport; (iii) again using intravital microscopy the local blood pressure in the original vasculature could be analyzed before implanting subcutaneously a small (radius <2 mm) tumour spheroid. Then the emerging spatial inhomogeneities of the tumour vasculature could be correlated with the spatially resolved blood pressure in the original vasculature.

In this work we were mainly interested in the morphological transformation of an arterio-venous initial vasculature by a growing tumour. Our intention was to characterize the complex geometry of the emerging networks and to identify the basic initial conditions and processes determining the emerging vessel network. There have been attempts to utilize such geometric characteristics of the tumour vasculature (like the fractal dimension) as a diagnostic tools in cancer research (Baish and Jain, 2000), but the purpose of our present work was not to extend these ideas. Rather, the messages that we intended to deliver were simply: (1) the initial vasculature *is* an important determinant of the tumour vessel network morphology and (2) the complex geometry and characteristic spatial inhomogeneities of the tumour vasculature emerges already from a few basic processes which we described here phenomenologically with stochastic rules.

Obviously one can pose the question, in how far our results depend upon our stochastic modelling approach. This describes certain processes on a coarser scale than *ab-initio* calculations (Frieboes et al., 2007; Bauer et al., 2007; Wise et al., 2008; Milde et al., 2008). For instance rather than calculating the solid stress within the tumour explicitly and incorporating it, among other factors, into the vessel collapse probability we use the prediction of continuum mechanical models for tumour growth (see, e.g. Breward et al., 2003) that solid stress is largest in the strongly proliferating periphery of the tumour and increase the collapse probability correspondingly in this region. Or rather than modelling adhesion forces between different cell species (ECs and tumour cells) and providing tumour cells with the capability to migrate, we do not involve migration and allow proliferation only when space and nutrients are available. Although we restricted ourselves in this paper to a parameter regime that leads almost exclusively to circular tumours a significantly enhanced nutrient demand of the tumour cells can also produce protrusions along the major vessels. Obviously, from a puristic modelling point of view it would be desirable to replace the phenomenological stochastic rules by deterministic processes involving solid stress, cell–cell adhesion and cell motility. But we think that we described the *effect* of these aspects on a sufficiently large scale correctly such that the main message (see above) will not change by a more detailed modelling, which is underway (to be published).

Besides these mechanical aspects there are important biochemical processes that we also modelled phenomenologically: (1) Instead of incorporating the negative feedback-loop involving VEGF receptors, Dll4 and Notch that restricts tip-cell generation during angiogenic sprouting (Bentley et al., 2008) we simply employed a rule, by which tip-cells can only be generated every 2nd or 3rd vessel segment (corresponding roughly 2–3 EC lengths). Such a rule is necessary when the initial vasculature is ubiquitous as in our model since otherwise the presence of VEGF generats tip-cells in an uncontrolled fashion. (2) Instead of modelling angiogenic sprout migration and branching involving matrix metalloproteases and collagen fibres (Bauer et al., 2007; Milde et al., 2008) we used commonly accepted stochastic rules (Anderson and Chaplain, 1998). The ubiquity of original vessels in our model diminishes the importance of the migration and branching process per se, since the intercapillary distances are rather short, which is different from models without initial vasculature. (3) We omitted an explicit mathematical description of the up-regulation of Ang-2 in ECs of coopted vessels within the tumour in Plank et al. (2004), but confined ourselves to describe only its destabilizing effect behind the tumour progresion front. (4) Similarly we did not model explicitly the up-regulation of EphB4 in tumour vessels that triggers the switch of the tumour vascularization program from angiogenic sprouting to circumferential growth but incorporated this switch with a heuristic rule.

Our intention in connection with the aspects 1–4 was to demonstrate that they have important consequences for the global morphology of the emerging tumour vasculature, and not to formulate a detailed ab-initio model for it. The simplifications were mainly motivated by computational tractability considerations for large scale simulations, in particular when transferring the model into a three-dimensional environment. In any case we would like to stress that if one would endeavour to implement a simulation environment that is expected to predict the growth of a particular tumour type in a specific tissue these aspects must be incorporated. In particular the geometry and characteristics of the initial vasculature has to be taken into account, which is missing in almost all existing tumour growth models. Not only the morphology of the emerging tumour vasculature is completely different in vessel-in-growth models (Anderson and Chaplain, 1998; Zheng et al., 2005; Frieboes et al., 2007; Wise et al., 2008; Milde et al., 2008) when compared with our results, but also their blood flow characteristics and their determinants for blood-borne drug transport are completely different (McDougall et al., 2002, 2006).

Hence the question remains, in which situations (or for what tumour types in which tissue) a vessel-in-growth model might be sufficient or whether the initial vasculature has to be taken into account. One has to consider that living tissue is always vascularized and that intercapillary distances for any tissue range from 50 to 150 μm. It appears therefore highly improbable that a tumour nucleus resides more than 200 μm away from the next capillary, and once it starts to grow parts of it will penetrate vascularized tissue. A pure vessel-in-growth situation is therefore only realized under artificial circumstances like in animal models (Gimbrone et al., 1974), and represents possibly a good approximation in cases where the tumour grows asymmetrically on a

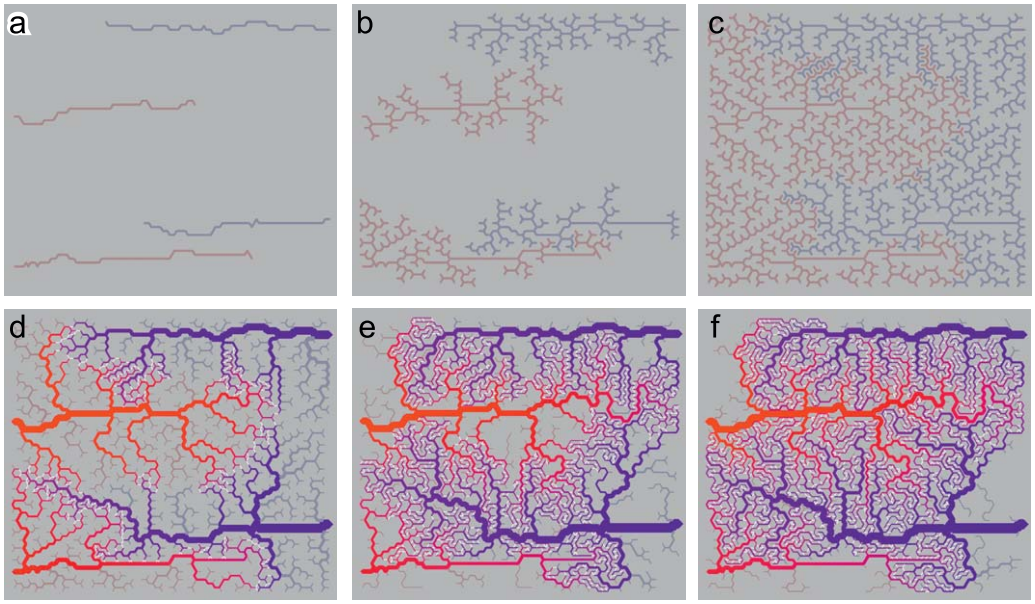

Fig. 15. Sketch of the construction method of vascular trees. The snapshots show a sample system, three times smaller than those needed for the simulation runs, during the growth stages. Arteries are shown in reddish tones, veins in blue. A dim colour indicates that no blood flow takes place. A saturated colour means that the vessel is perfused: (a) shows initial vessel chains randomly placed within specified bounds, (b) shows an intermediate configuration during the first stage where tripod elements are randomly attached to the tree tips, (c) shows the result of this stage, in (d) connecting capillaries (colour coded white) have been added as well as all vessel radii determined and blood flow computed. In between the perfused branches many other branches were unable to connect to their opposing type. Moreover the capillary distribution is concentrated half way between the major vessels, (e) shows an intermediate snapshot of the subsequenct optimization stage. Remodelling at the tree tips takes place based on the shear stress distribution. Weakly perfused vessel are removed, leaving space for growing heavily perfused vessels. Eventually this leads to a homogeneous capillary distribution in a well perfused network (f). (For interpretation of the references to colour in this figure legend, the reader is referred to the web version of this article.)

vascularized tissue sheet and extends perpendicularly into non-tissue region, as for instance in the dorsal skinfold chamber. In all other situations, in particular when tumours grow completely within well-vascularized tissues, an appropriate description of the surrounding tissue blood vessel network needs to be taken into account.

As we have mentioned before we have already generalized our model to a three-dimensional situation. Most aspects of the model can be transferred in a straightforward manner (Lee et al., 2006), only the construction of a three-dimensional arterio-venous network poses a non-trivial technical problem (to be published). We will also model O_2 release with associated intravascular O_2 decrease and replace the current discrete representation of tumour cells by a continuum description involving mechanical stress, tumour cell migration and cell–cell adhesion. For the study of drug-delivery within tumours in addition to blood-borne drug transport also extravasation and the interstitial fluid transport has to be incorporated into the model.

Appendix A

In this Appendix the construction of vascular trees is described.

The construction is based upon a small set of prescribed vascular stems from which arterio-venous trees will be grown. The basic structural element for this process is a tripod consisting of three vessel segments arranged in 120° angles. These tripods are appended successively at randomly chosen sites, either at the leafs of the growing trees or on the starting vessels. Thereby overlap with already occupied sites/bonds is forbidden, and so the process continues until there are no more valid configurations where tripods could be added. The resulting network consists of at least two binary trees with at least one arterial and one venous side (Fig. 15b, c).

To compute blood flow vessel radii must be known. "Murray's Law" (Murray, 1926) relates the radius of a parent vessel a_r to the radii of branches b_r, c_r. $a_r^\alpha = b_r^\alpha + c_r^\alpha$, where $\alpha = 2.7$ is a realistic value as used by Gödde and Kurz (2001). The radii of the tree leaves are set to 4 μm for arteries, and 5 μm for veins. Thus all other radii can be computed in a recursive algorithm which visits a vessel once its descendants have been processed.

To get a complete network, for each lattice bond a "capillary" vessel is added (3.5 μm radius) if it connects an arterial tree with a venous tree, if less than three vessels will connect to the nodes, and if all connected vessels fulfil $r < 20\,\mu m$.

Fig. 15d illustrates a sample configuration at this point before the second stage, in which the network is optimized by an iterative remodelling process. This consists of radius computation, capillary creation, flow rate and shear force computation, capillary removal, and the actual remodelling sweep, until the system reaches a steady state. Our remodelling sweep works as follows: an event type $E \in growth, death$ is drawn randomly for each segment according to the respective weights w_g, w_d. Relating these to shear stress f such that w_g is monotonically increasing and w_d is monotonically decreasing leads to expansion in well-perfused branches while non-perfused branches regress and make room for further growth. The details of the f dependence are not crucial. A linear mapping $\tilde{f} := (f - f_{min})/(f_{max} - f_{min})$ of the interval between the extremal values f_{min} and f_{max} over the vasculature usually suffices. Moreover we add a constant "offset" w_0 to both weights. This reduces the rate at which uncirculated vessels regress. And secondly it adds fluctuation to prevent deadlocks in high shear stress regions. Thus the final weights are $w_g = \tilde{f} + w_0$, $w_d = 1 - \tilde{f} + w_0$. Tree vessels are then traversed in random order.

An event E may take place but it can be rejected. This would be the case for the death of a segment in the middle of the tree since removal is restricted to the tree leaves. Growth happens at the downstream end of a vessel, not limited to leaves. It is rejected if there are already two daughter branches, or if the vessel radius

$r > 50\,\mu m$, or trivially if there are no unoccupied lattice sites. Else one of the admissible configurations is randomly picked. Beside tripods we also allow single vessel to be added. This facilitates growth into regions where bottlenecks evolved due to close proximity of two or more major vessels. Fig. 15e shows an intermediate step during stage. And Fig. 15f shows the final configuration.

References

Alarcon, T., Byrne, H., Maini, P., 2003. A cellular automaton model for tumour growth in inhomogeneous environment. J. Theor. Biol. 225, 257–274.

Ambrosi, D., Preziosi, L., 2002. On the closure of mass balance models for tumor growth. Math. Models Meth. Appl. Sci. 12, 737–754.

Anderson, A.R.A., Chaplain, M.A.J., 1998. Continuous and discrete mathematical models of tumor-induced angiogenesis. Bull. Math. Biol. 60, 857–900.

Baish, J.W., Jain, R.K., 2000. Fractals and cancer. Persp. Cancer Res. 60, 3683–3688.

Balding, D., McElwain, D.L.S., 1985. Mathematical modelling of tumour-induced capillary growth. J. Theor. Biol. 114, 53–73.

Bartha, K., Rieger, H., 2006. Vascular network remodeling via vessel cooption, regression and growth in tumors. J. Theor. Biol. 241, 903–918.

Bauer, A.L., Jackson, T.L., Jiang, Y., 2007. A cell-based model exhibiting branching and anastomosis during tumor-induced angiogenesis. Biophys. J. 92, 3098–3104.

Bentley, K., Gerhardt, H., Bates, P.A., 2008. Agent-based simulation of notch-mediated tip cell selection in angiogenic sprout initialisation. J. Theor. Biol. 250, 25–36.

Betteridge, R., Owen, M.R., Byrne, H.M., Alarcon, T., Maini, P.K., 2006. The impact of cell crowding and active cell movement on vascular tumour growth. Netw. Hetero. Media 1, 515–535.

Breward, C.J., Byrne, H.M., Lewis, C.E., 2003. A multiphase model describing vascular tumour growth. Bull. Math. Biol. 65, 609–640.

Brú, A., Albertos, S., Subiza, J.L., Lopez, J., García-Asenjo, Brú, I., 2003. The universal dynamics of tumor growth. Biophys. J. 85, 2948–2961.

Byrne, H.M., Chaplain, M.A.J., 1995. Mathematical models for tumour angiogenesis: numerical simulations and nonlinear wave solutions. Bull. Math. Biol. 57, 461–486.

Byrne, H.M., Preziosi, L., 2003. Modeling solid tumor growth using the theory of mixtures. Math. Meth. Biol. 20, 341–366.

Carmeliet, P., Jain, R.K., 2000. Angiogenesis in cancer and other diseases. Nature 407, 249–257.

Cassot, F., Lauwers, F., Fouard, C., Prohaska, S., Lauwers-Cances, V., 2006. A novel three-dimensional computer-assisted method for a quantitative study of microvascular networks of the human cerebral cortex. Microcirculation 13, 1–18.

Chaplain, M.A.J., Stuart, A.M., 1993. A model mechanism for the chemotactic response of endothelial cells to tumour angiogenesis factor. IMA J. Math. Appl. Med. Biol. 10, 149–168.

Chaplain, M.A.J., Giles, S.M., Sleeman, B.D., Jarvis, R.J., 1995. A mathematical model for tumour angiogenesis. J. Math. Biol. 33, 744–770.

Chaplain, M.A., 2000. Mathematical modeling of angiogenesis. J. Neurooncol. 50, 37–51.

Döme, B., Paku, S., Somlai, B., Tímár, J., 2002. Vascularization of cutaneous melanoma involves vessel co-option and has clinical significance. J. Path. 197, 355–362.

Drasdo, D., Höhme, S., 2005. A single-cell-based model of tumor growth in vitro: monolayers and spheroids. Phys. Biol. 2, 133–147.

Erber, R., Eichelsbacher, U., Powajbo, V., Korn, T., Djonov, V., Lin, J., Hammes, H.-P., Grobholz, R., Ullrich, A., Vajkoczy, P., 2006. EphB4 controls blood vascular morphogenesis during postnatal angiogenesis. EMBO 25, 628–641.

Frieboes, H.B., Lowengrup, J.S., Wise, S., Zheng, X., Macklin, P., Bearer, E., Cristini, V., 2007. Computer simulation of glioma growth and morphology. NeuroImage 37, 59–70.

Gerhardt, H., Golding, M., Fruttiger, M., Ruhrberg, C., Lundkvist, A., Abramsson, A., Jeltsch, M., Mitchell, C., Alitalo, K., Shima, D., Betsholtz, C., 2003. VEGF guides angiogenic sprouting utilizing endothelial tip cell filopodia. J. Cell Biol. 161, 1163–1177.

Gimbrone, M.A., Cotran, R.S., Leapman, S.B., Folkman, J., 1974. Tumor growth and neovascularization: an experiment model using the rabbit cornea. J. Nat. Cancer Inst. 52, 413–427.

Gödde, R., Kurz, H., 2001. Structural and biophysical simulation of angiogenesis and vascular remodeling. Dev. Dyn. 220, 387–401.

Griffon-Etienne, G., Boucher, Y., Brekken, C., Suit, H.D., Jain, R.K., 1999. Taxane-induced apoptosis decompressed blood vessels and lowers interstitial fluid pressure in solid tumors: clinical implications. Cancer Res. 59, 3776–3782.

Holash, J., Maisonpierre, P.C., Compton, D., Boland, P., Alexander, C.R., Zagzag, D., Yancopoulos, G.D., Wiegand, S.J., 1999a. Vessel cooption, regression, and growth in tumors mediated by angiopoietins and VEGF. Science 284, 1994–1998.

Holash, J., Wiegand, S., Yancopoulos, G., 1999b. New model of tumor angiogenesis: dynamic balance between vessel regression and growth mediated by angiopoietins and VEGF. Oncogene 18, 5356–5362.

Holmes, M.J., Sleeman, B.D., 2000. A mathematical model of tumour angiogenesis incorporating cellular traction and viscoelastic effects. J. Theor. Biol. 202, 95–112.

Holmgren, L., O'Reilly, M.S., Folkman, J., 1995. Dormancy of micrometastases: balanced proliferation and apoptosis in the presence of angiogenesis suppression. Nat. Med. 1, 149–153.

Jensen, H.J., 1998. Self-Organized Criticality: Emergent Complex Behavior in Physical and Biological Systems. Cambridge University Press, Cambridge.

Kim, E.S., Serur, A., Huang, J., Manley, C.A., McCrudden, K.W., Frischer, J.S., et al., 2002. Potent VEGF blockade causes regression of coopted vessels in a model of neuroblastoma. Proc. Natl. Acad. Sci. 99, 11399–11404.

Lee, D.S., Bartha, K., Rieger, H., 2006. Flow correlated percolation during vascular remodeling in growing tumors. Phys. Rev. Lett. 96, 058104-1–058104-4.

Liu, Z.J., Shirakawa, T., Li, Y., Soma, A., Oka, M., Dotto, G.P., Fairman, R.M., Velazquez, O.C., Herlyn, M., 2003. Regulation of Notch1 and Dll4 by vascular endothelial growth factor in arterial endothelial cells: implications for modulating arteriogenesis and angiogenesis. Mol. Cell. Biol. 23, 14–25.

Maisonpierre, P.C., Suri, C., Jones, P.F., Bartunkova, S., Wiegand, S.J., Radziejewski, C., Compton, D., McClain, J., Aldrich, T.H., Papadopoulos, N., Daly, T.J., Davis, S., Sato, T.N., Yancopoulos, G.D., 1997. Angiopoietin-2, a natural antagonist for Tie2 that disrupts in vivo angiogenesis. Science. 277, 55–60.

Macklin, P., McDougall, S., Anderso, A.R.A., Chaplain, M.J., Cristini, J., 2008. Multiscale modelling and nonlinear simulation of vascular tumour growth. J. Math. Biol. 58, 765–798.

McDougall, S.R., Anderson, A.R.A., Chaplain, M.A.J., 2006. Mathematical modelling of dynamic adaptive tumour-induced angiogenesis: clinical implications and therapeutic targeting strategies. J. Theor. Biol. 241, 564–589.

McDougall, S.R., Anderson, A.R.A., Chaplain, M.A.J., Sherratt, J.A., 2002. Mathematical modelling of flow through vascular networks: implications for tumour-induced angiogenesis and chemotherapy strategies. Bull. Math. Biol. 64, 673–702.

Milde, F., Bergdorf, M., Koumoutsakos, P., 2008. A hybrid model for three-dimensional simulations of sprouting angiogenesis. Biophys. J. 95, 3146–3160.

Mironov, V., Little, C., Sage, H. (Eds.), 1998. Vascular Morphogenesis: In Vivo, In Vitro, in Mente. Birkhäuser, Boston.

Murray, C.D., 1926. The physiological principle of minimum work: the vascular system and the cost of blood volume. Proc. Natl. Acad. Sci. USA 12, 207–214.

Nehls, V., Herrmann, R., Hühnken, M., 1998. Guided migration as a novel mechanism of capillary network remodeling is regulated by basic fibroblast growth factor. Histochem. Cell. Biol. 109, 319–329.

Owen, M.R., Alarcon, T., Maini, P.K., Byrne, H.M., 2008. Angiogenesis and vascular remodelling normal and cancerous tissues. J. Math. Biol. 58, 689–721.

Pahernik, S., Griebel, J., Botzlar, A., Gneiting, M., Dellian, M., Goetz, A.E., 2001. Quantitative imaging of tumour blood flow by contrast-enhanced magnetic resonance imaging. Brit. J. Canc. 85, 1655–1663.

Pezzella, F., Pastorino, U., Tagliabue, E., Andreola, S., Sozzi, G., Gasparini, G., et al., 1997. Non-small-cell lung carcinoma tumor growth without morphological evidence of neo-angiogenesis. Am. J. Path. 151, 1417–1423.

Plank, M.J., Sleeman, B.D., Jones, P.F., 2004. Lattice and non-lattice models of tumour angiogenesis. Bull. Math. Biol. 66, 1785–1819.

Pries, A.R., Reglin, B., Secomb, T.W., 2005. Remodeling of blood vessels: responses of diameter and wall thickness to hemodynamic and metabolic stimuli. Hypertension 46, 725–731.

Pries, A.R., Secomb, T.W., Gessner, T., Sperandio, M.B., Gross, J.F., Gaehtgens, P., 1994. Resistance to blood flow in microvessels in vivo. Circ. Res. 75, 904–915.

Pries, A.R., Secomb, T.W., Gaehtgens, P., 1995. Design principles of vascular beds. Circ. Res. 77, 1017–1022.

Sahani, D.V., Kalva, S.P., Hamberg, L.M., Hahn, P.F., Willett, C.G., Saini, S., Mueller, P.R., Lee, T.Y., 2005. Assessing tumor perfusion and treatment response in rectal cancer with multisection CT: initial observations. Radiology 234, 785–792.

Sainson, R., Aoto, J., Nakatsu, M.N., Holderfield, M., Conn, E., Koller, E., Hughes, C.C.W., 2005. Cell-autonomous Notch signalling regulates endothelial cell branching and proliferation during vascular tubulogenesis. FASEB J. 19, 1027–1029.

Sakariassen, P.Ø., Prestegarden, L., Wang, J., Skaftnesmo, K.O., Mahesparan, R., Molthoff, C., Sminia, P., Sundlisaeter, E., Misra, A., Tysnes, B.B., Chekenya, M., Peters, H., Lende, G., Kalland, K.H., Øyan, A.M., Petersen, K., Jonassen, I., van der Kogel, A., Feuerstein, B.G., Terzis, A.J., Bjerkvig, R., Enger, P.Ø., 2006. Angiogenesis-independent tumor growth mediated by stem-like cancer cells. Proc. Natl. Acad. Sci. 103, 16466–16741.

Scharpfenecker, M., Fiedler, U., Reiss, Y., Augustin, H.G., 2005. The Tie-2 ligand angiopoietin-2 destabilizes quiescent endothelium through an internal autocrine loop mechanism. J. Cell. Sci. 118, 771–780.

Stephanou, A., McDougall, S.R., Anderson, A.R.A., Chaplain, M.A.J., 2005. Mathematical modeling of flow in 2D and 3D vascular networks: applications to anti-angiogenic and chemotherapeutic drug strategies. Math. Comput. Model. 41, 1137–1156.

Stephanou, A., McDougall, S.R., Anderson, M.A.J., 2006. Mathematical modeling of the influence of blood rheological properties upon adaptative tumor-induced angiogenesis. Math. Comput. Model. 44, 96–123.

Stokes, C.L., Lauffenburger, D.A., 1991. Analysis of the roles of microvessel endothelial cell random motility and chemotaxis in angiogenesis. J. Theor. Biol. 152, 377–403.

Thompson, W.D., Shiach, K.J., Fraser, R.A., McIntosh, L.C., Simpson, J.G., 1987. Tumours acquire their vasculature by vessel incorporation, not vessel ingrowth. J. Path. 151, 323–332.

Torres Filho, I.P., Leunig, M., Yuan, F., Intaglietta, M., Jain, R.K., 1994. Noninvasive measurement of microvascular and interstitial oxygen profiles in a human tumor in SCID mice. Proc. Natl. Acad. Sci. USA 91, 2081–2085.

Turner, S., Sherratt, J.A., 2002. Intercellular adhesion and cancer invasion: a discrete simulation using the extended Potts model. J. Theor. Biol. 216, 85–100.

Vajkoczy, P., Menger, M.D., 2000. Vascular microenvironment in gliomas. J. Neurooncol. 50, 99–108.

Welter, M., Bartha, K., Rieger, H., 2008. Emergent vascular network inhomogeneities and resulting blood flow patterns in a growing tumor. J. Theor. Biol. 250, 257–280.

Wesseling, P., van der Laak, J.A., de Leeuw, H., Ruiter, D.J., Burger, P.C., 1994. Quantitative immunohistological analysis of the microvasculature in untreated human glioblastoma multiforme. Computer-assisted image analysis of whole-tumor sections. J. Neurosurg. 81, 902–909.

Williams, C.K., Li, J.-L., Murga, M., Harris, A.L., Tosato, G., 2006. Up-regulation of the Notch ligand delta-like 4 inhibits VEGF induced endothelial cell function. Blood 107, 931–939.

Wise, S.M., Lowengrup, J.S., Frieboes, H.B., Cristini, V., 2008. Three-dimensional multispecies nonlinear tumor growth—I model and numerical method. J. Theor. Biol. 253, 524–543.

Zhang, L., Yang, N., Park, J.W., Katsaros, D., Fracchioli, S., Cao, G., et al., 2003. Tumor-derived vascular endothelial growth factor up-regulates angiopoietin-2 in host endothelium and destabilizes host vasculature, supporting angiogenesis in ovarian cancer. Cancer Res. 63, 3403–3412.

Zheng, X., Wise, S.M., Cristini, V., 2005. Nonlinear simulation of tumor necrosis, neo-vascularization and tissue invasion via an adaptive finite-element/level-set method. Bull. Math. Biol. 67, 211–259.